

To Be Published by The Astronomical Journal (July 1, 2002)

Galaxies on the Blue Edge

J. E. Cabanela ¹

Haverford College, 370 Lancaster Ave, Haverford, PA 19041

jcabanel@haverford.edu

and

J. M. Dickey

*Astronomy Department, University of Minnesota
116 Church Street SE, Minneapolis, MN 55455*

john@astro.umn.edu

ABSTRACT

We have successfully constructed a catalog of HI-rich galaxies selected from the Minnesota Automated Plate Scanner (APS) Catalog of the Palomar Observatory Sky Survey (POSS I) based solely on optical criteria. We identify HI-rich candidates by selecting the bluest galaxies at a given apparent magnitude, those galaxies on the “blue edge” of POSS I color-magnitude parameter space. Subsequent 21-cm observations on the upgraded Arecibo 305m dish detected over 50% of the observed candidates. The detected galaxies are HI-rich with HI masses comparable to “normal” high surface brightness disk galaxies and they have gas mass-to-light ratios ranging from 0.1 to 4.8 (in solar units). Comparison of our candidate galaxies with known low surface brightness galaxies (hereafter LSBs) shows that they exhibit similar optical and HI properties to that population. We also show that previously identified LSBs, including several LSBs with red $B - V$ colors, preferentially occupy the “blue edge” of POSS I color-magnitude parameter space. Their presence on the “blue edge” appears to be a selection effect due to differing plate limits in the two POSS I bandpasses. This suggests the POSS I is a good filter for separating galaxies on the higher surface brightness end of the LSB population from the general population of galaxies in the night sky.

Subject headings: surveys, galaxies: peculiar, galaxies: statistics

1. Introduction

Low surface brightness galaxies (LSBs) are an important species of extragalactic object, differing from “normal” high surface brightness (HSB) galaxies in that their stellar disks are more diffuse (see Bothun, Impey, and McGaugh 1997). Their presence went largely unnoticed until the 1980s because they have central surface brightnesses lower than the sky surface brightness ($\mu_{sky} \approx 23$ mag/ \square'' in V). Disney (1976) demonstrated that most earlier galaxy catalogs had limiting surface brightnesses near the sky surface brightness and speculated that “what is seen above the sky background may be no reliable measure of what lies underneath.” This speculation proved correct in 1987 with the discovery of Malin 1 (Bothun, Impey, Malin, & Mould 1987), which appears as a small dwarf in short exposures on photographic plates (such as the POSS I), but reveals itself to be the largest known disk galaxy in deep exposures. Since then, many deep surveys have been conducted to investigate this previously unexplored population of LSBs.

A proposed explanation for the low surface brightness nature of LSBs is that they are probably very slowly evolving systems and have very low current star formation rates. This hypothesis is supported by the fact that while LSBs are typically HI-rich, their gas surface densities are observed to lie below the Toomre threshold for star formation over most of their gas disks (van der Hulst *et al.* 1993; de Blok, McGaugh, and van der Hulst 1996; van Zee 1999). The Toomre threshold density varies across a galaxy, and thus it is possible that while their densities are globally subcritical, there are regions of LSBs that temporarily meet the Toomre criterion for star formation, and thus some star formation occurs. Martin and Kennicutt (2001) cite examples of globally subcritical galaxies in which star formation is actually quite vigorous (e.g. NGC 2403 and M33). This theory could also explain why most LSBs are very blue, since most of the luminosity in these galaxies comes from a relatively few young stars, although the low metallicity of LSBs also appears to play a role (Gerritsen and de Blok 1999).

LSBs present a testbed for probing the evolution of stars and the ISM in low gas density environments. For example, it has been argued that Blue Compact Dwarfs (BCDs), HI-rich galaxies experiencing a current burst of star formation, are simply the cores of low surface brightness extended disks (Meurer *et al.* 1996). This potential relationship between BCDs and LSBs is contested (Salzer and Norton 1999), but it points out that we are still determining “what lies underneath” the sky brightness, so a large sample size is important to developing an understanding of the physical nature of these galaxies. There is thus strong motivation to construct a large catalog of LSBs and similar HI-rich galaxies.

One approach to finding these HI-rich galaxies has been blind radio surveys at $\lambda 21$ -cm (Schneider 1996; Briggs 1997; Dickey 1997; Staveley-Smith, Marquarding, Kilborn, & Webster 2001), which have the distinct advantage of not being affected by optical selection effects. However, blind radio surveys may be considered by some an inefficient use of resources due to the large amount of telescope time needed per detection obtained. Thus, despite the obvious selection effects, until recently, most HI-rich LSB galaxies were discovered through searches of wide-field optical surveys,

typically involving the visual examination of photographic plates to identify objects with low central surface brightness (See Schombert *et al.* (1992), Sprayberry, Impey, and Irwin (1996), and Impey and Bothun (1997) and the surveys cited therein). Followup is then performed at λ 21-cm in order to confirm a high HI content. Some semi-automated searches of photographic plates have also been performed. For example, Impey *et al.* (1996) used a combination of multiple optical parameters (including surface brightness) with visual followup in order to identify LSB candidates from the APM scans of UK Schmidt photographic plates. One limitation of searching photographic plates is that plate-based surveys can say nothing about the most diffuse LSBs, those below the plate limit. This problem was addressed in the CCD survey of O’Neil *et al.* (1997a) which has lower B surface brightness limits than photographic surveys, although a complete visual inspection of the images was necessary to identify LSB candidates. An automated mechanism for identifying LSBs or other HI-rich, low gas density galaxy candidates from wide-field optical surveys could certainly speed up the construction of a large catalog of LSBs. In addition, the automation could avoid the need for difficult to quantify subjective selection criteria for catalog members.

2. HI-rich Galaxies in Color-Magnitude Parameter Space

In a recent study of Hercules Cluster galaxies (Dickey 1997), we performed an λ 21-cm flux-limited survey of galaxies in four VLA fields (designated “NE,” “CE,” “SW,” and “47”) overlaying the Hercules cluster using the Very Large Array. The impetus for this initial study was to examine the HI properties of galaxies in the variety of environments present throughout the Hercules cluster. Motivated by an interest in possible optical counterparts to these HI-selected galaxies, we cross-identified the Dickey (1997) HI catalog (hereafter the Hercules HI catalog) with an optical catalog from the Minnesota Automated Plate Scanner Catalog of the POSS I (Odewahn *et al.* (1992); Pennington *et al.* (1993), hereafter the APS Catalog). The APS Catalog is constructed from digitized scans of both the blue 103a-O (hereafter O) and red 103-E (hereafter E) plates of the Palomar Observatory Sky Survey (POSS I). The APS Catalog can be distinguished from other digitized versions of the POSS I (such as the STScI Digitized Sky Survey) in part by the fact that each POSS I field was independently photometrically calibrated and both plates were scanned in each field, providing $O - E$ color information.

We obtained optical cross-identifications for 51 of the Hercules HI galaxies in the APS Catalog. For comparison, we also retrieved all the galaxies from the APS catalog in the four VLA fields covered in the Hercules HI study (a total of 7971 galaxies). All the Hercules catalog regions lie in a single POSS I field (P445¹), so plate-to-plate photometry zero-point variations do not affect the relative colors of these galaxies. We constructed a color-magnitude diagram using $O - E$ and E magnitude data for both the Hercules HI catalog and all the APS galaxies in the same areas

¹The POSS I field designations we use are the modified Luyten POSS I plate numbers, which are typically one greater than the plate reference numbers used in the Guide Star Catalog (Lasker *et al.* 1990).

(shown in Figure 1). It is evident from this diagram that the Hercules HI catalog galaxies are bluer than the majority of galaxies in the range $16 < m_O < 21$. Therefore most of the optical counterparts for this HI-selected sample of galaxies are on the “blue edge” of the color-magnitude diagram.

To more precisely quantify this effect, we define the “blue edge” boundary as the $O - E$ color separating the bluest 10% of galaxies of comparable E magnitude ($\pm 0.25^m$) in POSS I field P445 from the rest of the galaxies in that field. At brighter magnitudes, there are too few galaxies to define the blue edge in this manner, so we instead require the “blue edge” boundary to lie 0.3 magnitude redward of bluest galaxy. This boundary is fit with a 2nd order polynomial, such that

$$(O - E)_{BE} = \begin{cases} -10.172 + 1.4984m_E - 0.048391m_E^2 \\ 1.427 \end{cases} \text{ where } \begin{cases} m_E \geq 15.48 \\ m_E < 15.48 \end{cases} \quad (1)$$

where m_E is the extinction-corrected E magnitude of the galaxy.² We determined A_O and A_E for each galaxy in our sample using the E(B-V) maps from Schlegel, Finkbeiner, & Davis (1998) in conjunction with the UV to near-IR extinction law from Cardelli, Clayton, & Mathis (1989). We also tested extinction corrections based on the E(B-V) maps from Burstein and Heiles (1982) and found no substantial differences in our results.

The “blue edge” boundaries plotted on all the color-magnitude diagrams in this paper are defined by Equation 1. Using this definition of the “blue edge” boundary, we find over 80% of the Hercules HI galaxies lie blueward this “blue edge” boundary. Therefore, we speculated that this might be a property common to HI-rich galaxies, including the HI-rich LSBs. Consequently, an effective strategy for automatic optical selection of HI-rich candidates for an HI survey could be to simply observe the galaxies on the “blue edge” of POSS I color-magnitude parameter space.

3. Probing the “Blue Edge” of the Pisces-Perseus Supercluster

To test this hypothesis that “blue edge” galaxies are in general also HI-rich, we extracted a sample of such “blue edge” galaxies from the APS Catalog in the POSS I fields covering the Perseus-Pisces Supercluster. The Pisces-Perseus Supercluster (hereafter PPS) is one of the largest structures in the nearby universe. At a redshift between 4000 and 6000 km s^{-1} , the PPS and its surrounding filaments cover over 4000 square degrees of the sky, implying a linear extent of approximately $30h^{-1}$ by $50h^{-1}$ Mpc! The densest portion of the PPS, the “ridgeline” as defined by Cabanela and Aldering (1998), extends from (α, δ) of $(22^h, 40^\circ)$ through $(23^h, 28^\circ)$ to $(3^h, 40^\circ)$ (the region near the galaxy cluster A426). The extent of this supercluster is illustrated in Figure

²Due to variations in the photometry zeropoint from plate to plate, this equation for the blue edge is technically only valid for P445, although it should be a good estimate of the location of the “blue edge” boundary for most POSS I fields.

1 of Giovanelli, Haynes & Chincarini (1986) where it can also be seen that the PPS encompasses a very broad range of density environments, ranging from the high density regions of several rich clusters (including A262, A347, and A426) through a large volume with much lower densities, but higher than the field.

As noted by Giovanelli and Haynes (1985), the HI content of a galaxy can vary dramatically depending on its position relative to the cluster center. This is not simply a reflection of the established morphology-density relationship for galaxies (Dressler 1980), but rather is evidence that spiral galaxies suffer from HI stripping near cluster centers. A similar effect was seen by Dickey (1997) in the Hercules cluster, where extended HI disks are almost completely absent in galaxies in some regions but prevalent in others. HI stripping is seen to be a very efficient process in high density regions such as rich clusters (Cayatte, Kotanyi, Balkowski, & van Gorkom 1994). Consequently, while we will not directly investigate the efficiency of HI stripping here, the importance of surveying lower density environments is clear if we are to improve our odds of detecting galaxies with massive HI disks.

Our criterion for building a candidate list of potential HI-rich galaxies was to select APS Catalog galaxies on the “blue edge” of POSS I color-magnitude parameter space with apparent magnitude, m_E , between 16.0 and 21.0. We restricted our search to the portion of the sky within 2° of the PPS ridgeline defined by Cabanela and Aldering (1998) and within the declination range of the Arecibo telescope beam. This is a region west of the A426 and A262 with no obvious rich clusters. After removal of plate flaws and scratches identified by their spurious $O - E$ colors and E mean surface brightnesses, we selected the 30 bluest APS catalog galaxies in each 0.5 E magnitude-wide bin between E magnitude of 16.0 and 20.0. Using this criterion, we select the bluest 1% (or less) of the galaxies in each magnitude bin. From this initial list of 240 candidates on five POSS I fields (P293 through P297, see Table 1) we quickly performed a visual inspection of 125 of these candidates chosen to be the bluest galaxies at each E magnitude. The visual inspection of the POSS I prints allowed us to reject potential star–galaxy and star–star blended images (which are prevalent at low Galactic latitudes). Subsequent examination of POSS I image parameters of the “rejected” candidates showed they had higher surface brightnesses (lower mean μ_E values), and had smaller second moments, just as one would expect for stars. However, the “rejected” candidates were also typically fainter and smaller, most likely a result of the difficulty of classifying objects smaller than 0.1 mm in size on the plates by eye. Using this method, in one afternoon we reduced the subset of 125 candidates to 71 “clean” candidates for this HI search, hereafter referred to simply as the “blue edge” candidates (see Table 2) Several candidates are listed in the NASA/IPAC Extragalactic Database (NED); those cross-identifications are noted in Table 2.³

The PPS lies within 30° of the Galactic plane, so Galactic extinction is significant. Extinction corrections ranged from 0.15 to 0.35 magnitudes in the O bandpass and 0.09 to 0.19 magnitudes in

³The NASA/IPAC Extragalactic Database (NED) is operated by the Jet Propulsion Laboratory, California Institute of Technology, under contract with the National Aeronautics and Space Administration.

the E bandpass (see Table 2). Thus, we are probing an absolute magnitude range of roughly -18 to -13.5 in O, at the PPS distance, fainter than the measured M_* of -19.4 for the PPS (Cabanela and Aldering 1998). No k -corrections have been applied to any of the data presented in this paper as all the galaxies are below a redshift of $10,000 \text{ km s}^{-1}$ and any such corrections would be less than 0.1 magnitudes.

4. Arecibo Observations

We observed 31 of our “blue edge” candidates, as well as NGC 634 (for comparison to previous studies), with the 305m Arecibo telescope of the National Astronomy and Ionosphere Center over 14 nights between August 6 and August 20, 1998 in conjunction with another observing project (Cabanela and Dickey 1999).⁴ These observed “blue edge” candidates were chosen from the full list of 71 “blue edge” candidates (listed in Table 2), based only on their being accessible to the Arecibo beam during the observing run. The new Gregorian feed was used with the narrow L band receiver, resulting in a beam that is roughly oval in shape (depending on the zenith angle of the observation) with a FWHM of approximately $3'$.

4.1. Observational Methods

We obtained 21cm line spectra centered on the PPS mean velocity of 5000 km s^{-1} using staggered 25 MHz bands overlapping by 5 MHz, so that our final velocity coverage was 0 to $10,000 \text{ km s}^{-1}$ (1375 to 1420 MHz). The telescope and receivers performed very well, with a gain between 6 and 9 K Jy^{-1} and system temperature between 30 and 35 K depending on zenith angle. The spectra were calibrated using a previously measured gain function with zenith angle (provided by Phil Perillat).

Observations were taken in two on and off pairs, with 4 minutes of integration on the galaxy position followed by an equal integration on a reference position offset by 5 minutes in RA. The initial $\frac{\text{on-off}}{\text{off}}$ spectra for each target (resulting from 8 minutes on and 8 minutes off) was stored for later processing. Some candidates were reobserved and the multiple observations were co-added to reduce rms noise or to confirm a signal in the presence of strong radio frequency interference (RFI). In one case a galaxy was detected in the reference position, so we reobserved the target galaxy with the reference position taken earlier rather than later (negative offset in RA).

After total telescope time of about 16 minutes per galaxy (for single observations) we obtained spectra with rms noise of 18 mK in 24 kHz channels, giving a 3σ detection threshold of about $5 \times 10^7 M_\odot$ of HI per channel at 67 Mpc distance assuming the lowest gain of 6 K Jy^{-1} . Fourteen

⁴The National Astronomy and Ionosphere Center is operated by Cornell University under a cooperative agreement with the National Science Foundation.

of the 31 “blue edge” candidates observed were detected in HI and 4 were tentatively detected. These detections are detailed in Section 4.3.

4.2. Managing Radio Frequency Interference

Radio Frequency Interference (RFI) is the bane of extragalactic spectroscopy in the centimeter-wave band, particularly for single dish surveys like this one. Strong RFI can completely compromise an entire scan, but much more common is weak interference which is confined to a fairly narrow frequency range. These weak RFI signals can and do appear throughout our band. Some are fairly constant, and are thus easily distinguishable, while others are intermittent. Some appear and disappear in the on-source and off-source positions just as a real galaxy would. Some even reappear at roughly the same time on different days, so they can seem to be repeatable from day to day as a real galaxy must be. Thus it is not possible to definitively distinguish between a real extragalactic HI emission line and an interfering terrestrial signal by any means.

However, a very useful diagnostic for separating RFI from galaxy emission lines is the difference between the two circular polarizations. Since terrestrial interference is typically somewhat linearly polarized, any difference between the signal in the two polarizations identifies it as likely interference (*e.g.* - Schneider 1996). Our method for masking out interfering signals is based on an interactive task which displays the eight spectra (four bands times two polarizations) for each scan together, and then allows flagging of individual channels or channel ranges in one or both polarizations.

In addition to generating spurious detections, RFI consistently covered certain frequency ranges, which means that our non-detections must be qualified by details of which velocity ranges were not searchable due to consistent RFI. As an overall guide, Figure 2 shows the aggregate of all frequencies which were blanked due to interference in our entire run. These were determined for each source observation separately. Most spectra have three to five interference signals between 1375 and 1405 MHz. Figure 2 shows that the frequency range 1388.4 to 1388.6 MHz (6865 to 6910 km s^{-1}) is hardly ever usable, while the range from 1380 to 1382 (8300 to 8800 km s^{-1}) is often covered as well. These velocity ranges are therefore effectively excluded from our search.

In a few cases, it was difficult to determine whether we had observed weak RFI or a narrow emission line from a galaxy. In such cases we have tried to reobserve on different days to confirm the detection, but this was not always feasible. We class such observations as tentative detections (Group 3 in Table 3). It is also possible that interference can blend with a real galaxy detection to cause errors in the line integral, center velocity, and velocity width measurements. We indicate any such suspicious values for these measurements in Table 3.

4.3. Review of Detected Galaxies

Of the 31 “blue edge” candidates we observed, 19 (or 61%) are detected (or tentatively detected) in HI. In addition to these 19 detections, we detected an additional three galaxies in off-scans and obtained a serendipitous detection of UGC 630 in the field of MAPS-P295-1915216.⁵

The detected galaxies were divided into five groups to aid in the initial analysis. Group 1 consists of HI detections with high signal-to-noise ratios and contains 14 of our HI galaxies and the serendipitously observed galaxy, UGC 630 (see Figure 3). Group 2 consists of positions around MAPS-P295-1369071, which were repeatedly observed in order to confirm that our detection is not confused by another galaxy on the edge of the field with the Arecibo beam (see Figure 4). Group 3 contains the four tentative HI detections (see Figure 5). Group 4 consists of the three galaxies we detected in the off-scans of our galaxies (see Figure 6). And group 5 contains NGC 634, which was observed for comparison with previous observations. We discuss the detected galaxies individually below.

The 3' Arecibo beam does not resolve the galaxies and thus provides no direct information on the rotation curves of these HI disks. Our goal has been detection, not high-resolution HI imaging. However, many dwarf galaxies which have been mapped with aperture synthesis telescopes show rising rotation curves, not only throughout their optical disks, but throughout their HI extent as well (Taylor *et al.* 1996). In the extreme case of a solid body rotation curve throughout the HI disk, the resulting single dish spectrum should have a semi-circular or semi-elliptical shape, with a single peak at the center velocity. If the rotation curve flattens at large radii this shape changes to the familiar “two-horned” profile, with two peaks at the two velocity extrema of the line, which correspond to the projected rotation velocities of the two ends of the major axis (e.g. Lavezzi and Dickey 1997). Most of our observed galaxies have profiles which have a square-top or two-horned shape, suggesting that their rotation curves are flattening at large radii. This needs to be confirmed with aperture synthesis mapping.

Our individual observations are detailed below, in the order in which they appear in Table 3.

MAPS-P293-268610: This galaxy was observed twice. The first time its spectrum was confused by emission from the galaxy UGC 105 in the reference position. We reobserved it the following day, with the reference spectrum taken at $\alpha - 5^m$ instead of $\alpha + 5^m$, to sort out the two profiles. In fact there is no overlap in velocity between the two galaxies, so we have averaged the two observations here, blanking the channels below 8250 km s^{-1} which are covered by UGC 105. The profile appears to have two peaks (“horns”) with sharp edges on either side from which we may infer that this is a rotating gas disk with a rotation curve which flattens at large radii. This inference assumes a “typical” HI surface density profile for a disk galaxy and will require confirmation via aperture synthesis observations.

⁵The IAU designation of objects in the Minnesota Automated Plate Scanner Catalog indicates the POSS I field number, in this case P295, and the unique O plate “starnum” identifying that object in that field, in this case 1915216.

MAPS-P293-100987: This galaxy, also identified as F409-05 from Eder *et al.* (1989), shows a two-horned profile shape, indicating an extended, flat rotation curve in the outer regions (assuming an HI distribution as seen in disk galaxies). While our velocity, 4851 km s^{-1} , is consistent with the velocity of 4864 km s^{-1} reported by Eder *et al.* (1989), our gas mass, $1.8 \times 10^9 M_\odot$, is a bit lower than the value of $2.26 \times 10^9 M_\odot$ we compute from Eder *et al.*'s data.

MAPS-P293-249758: This galaxy was observed twice on different days, and the results are consistent, however on both days there appears to be a narrow interference spike near the center of the line profile. The presence of this interference in the middle of such a faint line raises the concern that the entire profile may be interference generated, either by sidebands of the signal or by the spectrometer resolving function. However that interference signal is present throughout the entire night of observing on both days, and it never shows width of more than about four channels (1388.5 to 1388.6 MHz). So although our measurements of this profile suffer from uncertainty due to the necessity of masking these channels in the middle of the presumed galactic line, we are moderately confident of the detection.

MAPS-P293-179271 This clearly detected line comes from a very faint galaxy, whose optical image is almost blended with a pair of bright stars. The line profile is single peaked, which suggests a disk with a solid body rotation curve, a face-on orientation, or perhaps a turbulent cloud of gas.

MAPS-P294-727319: This faint, diffuse galaxy has an extremely bright HI line, which indicates a gas mass of roughly $2 \times 10^9 M_\odot$. Yet the line is centrally peaked, which implies that it comes from a cloud or disk which does not have a flat rotation curve, but may be more or less in solid body rotation. A warped disk is one possible explanation of the line shape, although confirmation will, again, require aperture synthesis observations.

MAPS-P295-699736: This is a strong and very well detected line. We repeated the observation on two different days with consistent results, and there is no interference nearby in frequency on either day. Optically the galaxy is extended, but everywhere low in surface brightness, just above the plate limit in both colors. This is a good example of a massive gas disk with very low optical luminosity.

MAPS-P293-1790367: This galaxy was observed twice, with consistent results between the two days. There is a suggestion of two “horns”, but these may correspond to two systems which appear separate on the optical image.

MAPS-P295-823940: This galaxy was observed on two different days, with consistent results. However the second day's observations were compromised by interference on the low velocity side of the galaxy (5250 to 5350 km s^{-1}). Such a narrow, single-peaked profile could easily be generated by an interfering signal. We have moderate confidence that this does represent a detection, but there is a significant chance (perhaps 10 percent) that we are being fooled by an interference signal.

MAPS-P295-1693362: This relatively bright galaxy (cross-identified in NED as CGCG 501-047) shows a very clear two-horned profile shape. The gas disk probably has an extended, flat

rotation curve in the outer parts. The optical image has a bright nucleus and an extended disk.

MAPS-P295-1915216: The spectrum in this direction shows two emission features which look like galaxies. The stronger one (at 4878 km s^{-1}) has a classic two-horned shape, indicating a disk in circular rotation with a rotation curve which flattens at the outer edges. The second feature (at 6786 km s^{-1}) is weaker, but still very well detected above the noise. The optical image shows a relatively large galaxy (identified in NED as UGC 630) about an arc minute to the west of the blue dwarf which was our target. UGC 630 has a measured redshift of 4884 km s^{-1} (Schneider *et al.* 1990), we therefore identify the other (6786 km s^{-1}) line with MAPS-P295-1915216.

MAPS-P295-642385: This galaxy was observed on two different days, with consistent results. On one day there was interference at higher velocities (4850 to 5000 km s^{-1}), but the second day is very clean in this area, so we are very confident of the detection. The line is very narrow and single-peaked, which suggests solid body rotation throughout the HI, if there is a disk in circular rotation. Several faint, diffuse images appear to the south west of the galaxy, all within the beam area, so the correspondence of the line with the central object is in some question.

MAPS-P295-1202937: This is a very strong detection of an extremely faint galaxy. The line profile is clearly two-peaked, corresponding to an extended disk of gas. We have not had time to map around this position, but there seem to be no alternative galaxies in the vicinity which could account for the observed gas.

MAPS-P295-1326244: This is a very narrow line from a relatively bright galaxy. The detection is somewhat tentative as we have not had time to confirm it with a reobservation. The narrow width makes it somewhat more likely than most of our detections to be interference. Assuming it is real, the shape of the profile suggests either a disk seen nearly face on, or one with a solid-body rotation curve.

MAPS-P295-910484: This strong line is a clear-cut detection of this diffuse, blue galaxy. The sharp edges on the line, and the suggestion of two peaks, imply an extended disk of gas with a rotation curve which flattens at the edges.

MAPS-P295-1369071: This strong line was observed only on one day, but it is far from any interference and the detection is quite solid. The line shape suggests a disk with an extended, flat rotation curve. The mass of gas in this galaxy is so high, and its optical luminosity so low, that we have searched the vicinity of the object to confirm that the gas cloud is centered on the optical candidate. We observed three other positions, one on either side of this object offset by $1.3'$, and one centered on the nearby galaxy NPM1G $+30.0027$. The results confirm that this faint blue galaxy is the center of the HI cloud. The spectra on either side have similar profiles, but weaker by about a factor of 0.6, as expected given the beam shape. The emission toward NPM1G $+30.0027$ is much fainter yet. Thus the identification of this line with the faint blue galaxy MAPS-P295-1369071 appears to be conclusive. The extended Arecibo observations also allow us to determine that the direction of the galaxy's spin vector is northward. The relationship among these beam centers and their corresponding spectra are illustrated on Figure 4.

MAPS-P295-2259922: This galaxy exhibits is a very weak line. It appears at about the five sigma level in two different observations taken on two different days. The results of the two are consistent within the errors. On neither day is there obvious interference at this frequency, although on the first day there is interference at somewhat higher velocity (6000 km s^{-1}). We have confidence that this is a real emission line, but given its low signal-to-noise we class it as a tentative detection.

MAPS-P295-83632: This is a very tentative detection, the most questionable of all of our “lines.” The profile resembles a weak interference feature. Although the signal-to-noise ratio is good, we are very hesitant to identify this feature as real HI emission because of its narrow width and very sharp edge. We have not had time to follow-up with a reobservation on a second day.

MAPS-P295-773634: This weak line is a very tentative detection. It was observed only once, we did not have time to return for another observation on another day. The line appears identically in both polarizations, and there is no interference nearby. The baseline is quite flat, so it is unlikely that this could be an artifact of the receiver or spectrometer. However the line is near the radiometer noise limit, so its parameters cannot be well measured.

MAPS-P295-576122: This weak line is a very tentative detection. It was observed only once. There is a narrow interference feature about 150 km s^{-1} higher, but it seems to be confined to an extremely narrow band. We have not had time to reobserve this position to confirm the detection.

UGC 105: Detected in the reference beam for MAPS-P293-268610. We found HI associated with UGC 105, $78''$ from the reference beam center. Its identification is supported by the match of our velocity to the velocity of 8046 km s^{-1} from the Third Reference Catalogue of Bright Galaxies (de Vaucouleurs *et al.* (1991), hereafter RC3) catalog (de Vaucouleurs *et al.* 1991).

MAPS-P293-102675: A serendipitous detection in the reference beam, a relatively bright galaxy $50''$ from the reference position of MAPS-P293-100987 appears to have been detected, as there are no other likely candidates in the field of the reference beam.

MAPS-P294-444433: An apparent serendipitous detection at the reference position of MAPS-P295-1577104, this curious feature appeared as a pair of negative lines in our observation of this galaxy. It is in a fairly interference-free region of the band, although there is a narrow spike about 100 km s^{-1} higher in velocity than the center of the higher velocity emission line. The nearest galaxy to the reference position of the observation appears to be MAPS-P294-444433, located $83''$ from the beam center. The detection is only tentative, and not obviously is associated with the galaxy, but it is worthy of follow-up observations. If it is real, it may represent either two objects, or a disk or ring of gas.

NGC 634: We observed this galaxy as a test of the system. It has been described before by Wegner, Haynes, & Giovanelli (1993) and by Theureau *et al.* (1998). The central velocities in the literature are 4942 and 4925 km s^{-1} , we find 4916 km s^{-1} , which is in good agreement, given the broad HI line width. Wegner, Haynes, & Giovanelli (1993) find widths of 520 km s^{-1} at 50% of the mean and 492 km s^{-1} at 20% of the peak versus our measurement of 512 km s^{-1} . We measure

4.5 Jy-km s⁻¹ for the line integral; Theureau *et al.* (1998) find 4.3 Jy-km s⁻¹ but Wegner, Haynes, & Giovanelli (1993) find 6.8 Jy-km s⁻¹. Thus our calibration seems to be in rough agreement with earlier work, although the range of values for the line integral is a bit worrisome.

5. HI Properties of the “Blue Edge” Galaxies

The HI masses of our (detected) “blue edge” galaxies range from $2.7 \times 10^8 M_{\odot}$ to $3.6 \times 10^9 M_{\odot}$.⁶ These gas masses fall about 1 dex below the turnoff in the HI mass function (Schneider 1996), but on the high end of the gas masses typically seen for dwarf irregulars such as the SMC (Skillman 1996). This is consistent with their integrated HI spectral profiles, which generally show two-horned profiles typical of galaxies with flat rotation curves. Such flat rotation curves are common for larger spirals and LSBs (Verheijen and Sancisi (2001) and references therein) as opposed to dwarf galaxies, whose rotation curves typically rise throughout their disks (Taylor *et al.* 1996).

In order to estimate the gas mass-to-light ratios of our “blue edge” galaxies, we compute the distance modulus as

$$m - M = 25 - 5 \log H_0 + 5 \log cz + 1.086(1 - q_0)z \quad (2)$$

(Weinberg 1972), where we assume $H_0 = 72$ km s⁻¹ and $q_0 = 0.5$. No corrections have been made for Virgo infall or internal extinction. Using this definition of the distance modulus, we find that our “blue edge” galaxies have gas mass-to-light ratios, M_{HI}/L_O , of 0.09 to 4.79 in solar units. If $M_{\text{HI}}/L_O \approx M_{\text{HI}}/L_B$, this indicates most of our “blue edge” galaxies have gas mass-to-light ratios considerably higher than typical HSB spiral galaxies, which have M_{HI}/L_B typically below 0.60 (in solar units) (Roberts and Haynes 1994; Maia, Willmer, & Da Costa 1998). Such high gas mass-to-light ratios are typical of LSBs (Impey *et al.* 1996; O’Neil *et al.* 1997a). This suggests our “blue edge” galaxies may have HI properties common to LSBs, something we will investigate more thoroughly in Section 6.

Before continuing, we briefly address an issue we mentioned in Section 3: the possibility of HI stripping in galaxies near the PPS ridgeline. The HI mass deficiency of galaxies is known to correlate with environmental density (Giovanelli and Haynes 1985). Although we do not have density estimates for the PPS per se, we previously defined a high surface density “ridgeline” based on the distribution of ZCAT galaxies in the PPS field (Cabanela and Aldering 1998). Because the PPS is oriented edge-on (Giovanelli and Haynes 1988), angular distances from the ridgeline correspond to distances from the highest density portions of the PPS. Our investigation finds no correlation between HI mass and angular distance from the PPS ridgeline (see Figure 7a). A very weak correlation ($r = 0.26$) between the HI mass to light ratio, M_{HI}/L_O , and angular distance

⁶We do not attempt to derive the dynamical masses for our “blue edge” galaxies because the resolution of the POSS I plates for images this small results in large uncertainties in the galaxy’s inclination angle.

from the ridgeline is observed (Figure 7b). The best-fit line describing this correlation is

$$M_{\text{HI}}/L_O(r_d) = 0.613(\pm 0.564) \times r_d + 1.750(\pm 0.061), \quad (3)$$

where r_d is the ridgeline distance in degrees. However, the best-fit slope is only 1.1σ from a value of zero, there is a significant likelihood there is no correlation at all.

6. Are the “Blue Edge” Galaxies a Distinct Population?

This project started with the realization that the majority of the optical counterparts to the HI-selected galaxies from Dickey (1997) lay on the “blue edge” of the POSS I color-magnitude diagram for galaxies. Our HI observations show the converse is also true: many “blue edge” galaxies appear to be HI-rich. This leads us to ask in what other ways these “blue edge” galaxies are distinct from the “normal” HSB galaxy population (other than being bluer)? The answer, as we will show, is that the 19 “blue edge” galaxies we detected in HI (those in Groups 1, 2, or 3) are clearly a distinct population from “normal” HSB galaxies in both their optical and HI properties. We support our claim using several previously published HSB and LSB galaxy catalogs (Table 4) to construct four major pieces of evidence which we will outline in this Section. First, the bivariate brightness distributions of our “blue edge” galaxies are more similar to those of LSBs than HSBs. Second, known LSBs appear as “blue edge” galaxies on the POSS I. Third, the HI masses of our “blue edge” galaxies are much lower than typical HSB galaxies, but typical of known LSBs at comparable redshifts. And finally, the gas mass to light ratio of our “blue edge” galaxies are similar to known LSBs of similar POSS I color.

6.1. The Bivariate Brightness Distribution of “Blue Edge” Galaxies

Driver and Cross (2000) suggest an approach to classifying galaxies based on their positions in a bivariate brightness distribution (hereafter BBD) plot, a plot of mean surface brightness versus absolute magnitude. They use this approach to show that the traditional Hubble sequence of galaxies segregates reasonably well into different regions of this parameter space. Furthermore, non-Hubble sequence galaxies such as LSBs and cDs are easily accommodated on the BBD plot and appear isolated from Spirals and Ellipticals. Thus, a BBD plot provides a simple means of comparing the optical properties of the “blue edge” galaxies we observed with those of previously identified HSB and LSB galaxies. With this goal in mind, we cross-identified several galaxy catalogs containing redshifts with the APS catalog (those listed under the “BBD” column of Table 4). Correcting the O magnitudes (but not diameters) for Galactic extinction as outlined in Section 2, we estimated the absolute O magnitude (using equation 2) and mean O surface brightness for each comparison galaxy.

A BBD of our “blue edge” galaxies and a large sample of “normal” HSB galaxies in the PPS field extracted from the CfA Redshift Catalog (hereafter ZCAT, Huchra *et al.* (1992)) clearly shows

that the two populations differ (See Figure 10). We can account for the fact that our “blue edge” galaxies are intrinsically fainter than the ZCAT by noting that while not explicitly flux-limited, the ZCAT contains mostly bright galaxies with $O < 17$. However, our “blue edge” galaxies are also lower surface brightness than the ZCAT galaxies. This is intriguing since surface brightness was not a criterion for identifying “blue edge” galaxies. By adding POSS I data for LSB galaxies identified from another plate-based survey (Impey *et al.* 1996) and a CCD-based survey (O’Neil *et al.* (1997a), hereafter OBC) to our previous BBD plot, we find that our “blue edge” galaxies lie on the high luminosity end of the LSB population in the BBD plot. This implies “blue edge” galaxies are very similar galaxies to the LSBs seen on the POSS I (Figure 11).

6.2. Known LSBs in POSS I Color-Magnitude Parameter Space

Driven by the fact that the BBD of our “blue edge” galaxies overlaps with that of known LSBs, we now examine the POSS I color-magnitude distributions of previously identified LSBs, including several from LSB catalogs with no redshifts available (see the “color-magnitude” column of Table 4). A plot of the color-magnitude distribution of these LSBs shows that the majority of them also lie along the “blue edge” (see Figure 8). We quantify this by defining the color difference from the “blue edge” boundary as

$$\Delta(O - E)_{BE} = (O - E) - (O - E)_{BE} \quad (4)$$

where $(O - E)$ is the extinction corrected $O - E$ color of the galaxy and the $(O - E)_{BE}$ is defined by equation 1. Using equation 4, we determine the cumulative $\Delta(O - E)_{BE}$ distributions for each of these LSB galaxy catalogs (Figure 9). All these catalogs show $\Delta(O - E)_{BE}$ distributions very different from the general POSS I galaxy population, but quite similar to each other. Whereas only 10% of APS catalog galaxies have $\Delta(O - E)_{BE} < 0$ (by definition), over 68% of LSBs galaxies lie blueward of the “blue edge” boundary! Surprisingly, this is even the case for the LSBs from the OBC catalog, which includes many LSBs with red $B - V$ colors. This apparent discrepancy will be addressed in Section 7.

The maximum difference of the cumulative $\Delta(O - E)_{BE}$ distributions between datasets can be used as a Kolmogorov–Smirnov (K–S) D statistic to compute the likelihood that the datasets were drawn from the same parent distribution (see Press *et al.* (1992)). Such K–S tests indicate that these LSBs have probabilities of less than 10^{-15} of being drawn from the same $\Delta(O - E)_{BE}$ distribution as the POSS I galaxies (See Table 5). This doesn’t mean that all these LSBs have identical $\Delta(O - E)_{BE}$ distributions (a quick examination of Table 5 shows they don’t), but they are clearly all drawn from populations that lie preferentially on the “blue edge” of POSS I color-magnitude parameter space.

6.3. Comparison of HI Properties with Known LSBs

We now compare the HI properties of our “blue edge” galaxies (as outlined in Section 5) with those of three other galaxy catalogs: a high surface brightness catalog of bright galaxies (the RC3) and two LSB catalogs (see the “ M_{HI} ” column of Table 4). Since a given radio flux limit will result in a varying minimum HI mass limit with varying redshift, we restrict the comparison galaxies to the observed range of redshifts of our “blue edge” galaxies ($4000 \text{ km s}^{-1} < cz < 9000 \text{ km s}^{-1}$). To ensure that our comparison samples are not biased toward fainter galaxies, we also require that they exhibit the same optical flux limit of $m_E < 20$ as the “blue edge” galaxies. Applying these restrictions results in relatively small comparison samples of LSBs (see Table 4), but ensures they have similar optical flux and HI mass limits.

Our “blue edge” galaxies exhibit M_{HI} values peaked around $\log(M_{HI}) \sim 9.0$. This peak lies roughly 0.8 dex below the peak observed for HSB galaxies from the RC3, but lies in the range of the M_{HI} values seen for LSBs (Figure 12a). We quantify the level of resemblance between these distributions of M_{HI} values by using K–S tests to compare them (see Table 6). As expected based on Figure 12, our “blue edge” galaxies have an M_{HI} distribution that is most similar to the LSBs, with the OBC galaxies having an 88% chance of being drawn from the same parent M_{HI} distribution. This stands in marked contrast to the HSB galaxies in the RC3, which have only a probability of 3×10^{-10} of sharing the same parent M_{HI} distribution as the “blue edge” galaxies. Clearly, based on these small samples, our “blue edge” galaxies share more in common with LSBs than HSBs where there gas masses are concerned.

In retrospect, this should not be a very surprising result. If galaxies exhibit a limited range of gas mass-to-light ratios, we expect that the more luminous galaxies will tend to have higher total gas masses. This expectation is confirmed in a plot of M_{HI} versus L_O for these galaxies (Figure 13). The RC3 galaxies all lie at relatively high luminosities and have correspondingly high M_{HI} values. Our “blue edge” galaxies lie at the low luminosity, low gas mass edge of the RC3 distribution. Their distribution does not extend to the very lowest luminosities seen for LSB galaxies. Notably, the distribution of M_{HI} versus L_O for these galaxies has a slope less than one, indicating higher gas mass-to-light ratios for less luminous galaxies, an observation previously made by Staveley-Smith, Davies, and Kinman (1992). A separate examination of the M_{HI}/L_O distribution of our “blue edge” galaxies reveals it is peaked around $\log(M_{HI}/L_O) \sim 0.25$ (Figure 12b). This is significantly higher than the peak M_{HI}/L_O for the RC3 galaxies (~ 0.5 dex higher) but appears to be roughly equal to the peak of the distributions for the LSBs. This is supported by K–S tests comparing the distributions which show both LSB catalogs have a 20% or greater chance of sharing the same gas mass-to-light distribution as our “blue edge” galaxies, while the HSB galaxies from the RC3 show only a 0.3% chance. On the other hand, it appears that our “blue edge” galaxies lack the extremely high M_{HI}/L_O galaxies seen in LSB catalogs (as seen in Figure 13), though this conclusion is based on a population of only 19 “blue edge” galaxies.

We might be able to explain this bias against extremely high M_{HI}/L_O “blue edge” galaxies by

considering that color and M_{HI}/L_O may be correlated. Bothun (1984) found that the M_{HI}/L_B of late-type spirals was correlated with $B - V$ and even more strongly with $B - H$. Bothun ascribed these correlations to a relationship between the initial star formation rate (SFR) of the galaxy and its subsequent evolution (Bothun 1982). The better correlation using infrared bandpasses was attributed to the fact that blue luminosities of galaxies are more affected by uncertain levels of internal extinction. Giraud (1987) instead argues that the better correlation using infrared bandpasses is because H bandpass luminosity depends on an older population of stars than B bandpass luminosity and thus M_{HI}/L_H is a measure of the present HI reservoir of the galaxy versus its star formation history (rather than its current SFR). More recently, Matthews and Gallagher (1997) find that for extreme late-type galaxies, the blue galaxies all have high M_{HI}/L_V , while red galaxies exhibit a broad range of gas mass-to-light ratios. Matthews and Gallagher suggest that this broad range in M_{HI}/L_V for red galaxies is because some galaxies with older stellar populations retain large HI reservoirs in their outer disks, where surface densities drop below the Toomre criterion for star formation to occur.

Using the four catalogs cited above (see the M_{HI} column of Table 4), we construct a plot of M_{HI}/L_O versus $O - E$ (see Figure 14). This plot reveals a trend similar to that cited by Matthews and Gallagher (1997) in that redder galaxies tend to have a wider distribution of M_{HI}/L_O than blue galaxies. From this plot, it is clear our “blue edge” galaxies mark the bluest end of a flared distribution of M_{HI}/L_O versus $O - E$. From this plot, we see that the LSBs reaching gas mass-to-light ratios much higher than our “blue edge” galaxies are all relatively red. And from examining this diagram, we see our “blue edge” galaxies lie in a region dominated by very blue LSBs which have a very similar range of smaller M_{HI}/L_O ratios. In a model proposed by Matthews and Gallagher (1997), this suggests our galaxies have a lower likelihood of having large untapped HI reservoirs in their outer disks than the redder LSBs.

6.4. The “Blue Edge” Galaxies as LSBs

Classifying a galaxy as a *bona fide* LSB traditionally requires deep images to assess its surface brightness profile to see if it meets specified “low surface brightness” criterion. Without such images for our “blue edge” galaxies, we can not absolutely verify their LSB nature. However, we assert that our “blue edge” galaxies as a population seem very similar to LSBs in most respects. Most previously identified LSBs visible on the POSS I lie on the “blue edge” of POSS I color-magnitude parameter space. The bivariate brightness distribution of “blue edge” galaxies appears relatively similar to that of known LSBs on the POSS I. Furthermore, the HI properties of our “blue edge” galaxies exhibit similar M_{HI} distributions to LSBs at similar redshifts. If we take into account the relationship between M_{HI}/L_O and $O - E$ (Figure 14), it is clear that our “blue edge” galaxies exhibit very similar gas mass-to-light ratios as blue LSBs. Thus, despite the fact that low surface brightness was not an explicit selection criterion for identifying the “blue edge” galaxies, the evidence at hand suggests that our “blue edge” galaxies share much in common with

the LSBs visible on the POSS I. Of course, the relatively high surface brightness limit of the POSS I means LSBs visible in that survey are likely to represent the high surface brightness end of the LSB population. Thus, we would be safer to identify our “blue edge” galaxies as similar to the high surface brightness end of the LSBs.

7. Understanding the “Blue Edge”

The fact that LSBs lie on the “blue edge” of color-magnitude parameter space is not surprising, since LSBs are observed to be very blue (Bothun *et al.* 1997; Impey and Bothun 1997). Thus, given our selection criterion for “blue edge” galaxies it is plausible that we are selecting blue HI-rich LSBs. However, the preponderance of blue LSBs has been questioned by O’Neil and collaborators who recently performed a CCD-based search for LSBs (O’Neil *et al.* 1997a) and discovered several LSB galaxies with red $B - V$ colors. O’Neil *et al.* (1997b) suggest that the observed preponderance of blue LSBs is a selection effect due to the blue sensitivity of photographic plates used in most previous optical LSB searches. Therefore it was surprising that our cross-identification of the 73 OBC galaxies on the POSS I fields which were online in the APS Catalog in August 2000 recovered 58 of them. Furthermore, these OBC galaxies are predominantly on the “blue edge” of the POSS I color-magnitude space (as seen in Figure 9). Are we truly seeing LSBs with “red” $B - V$ on the “blue edge?”

7.1. Red LSBs on the “Blue Edge”?

If we assume, as O’Neil *et al.* (1997b) do, that the blue sensitivity of photographic plates is a strong selection effect, then a cross-identification of the OBC with the POSS I would preferentially match only the bluest galaxies in the OBC survey. However, a plot of $B - V$ vs. V for OBC galaxies separated into matched and unmatched galaxies shows the APS Catalog does not preferentially match the bluest OBC galaxies (see Figure 15a). While the average $B - V$ color of the unmatched galaxies is slightly redder ($\langle B - V \rangle = 0.78 \pm 0.01$) than that of matched galaxies ($\langle B - V \rangle = 0.82 \pm 0.02$), the $B - V$ color distribution of the matched galaxies extends both blueward and redward of that of the unmatched galaxies. Instead, it appears the dominant bias in the POSS I is that it doesn’t recover the lowest surface brightness OBC galaxies (Figure 15b). If we can understand how OBC galaxies with “red” $B - V$ colors can appear on the “blue edge” of POSS I color-magnitude parameter space, we may have an explanation for why LSBs appear on the “blue edge.”

A plot of $O - E$ vs. $B - V$ shows that these two colors appear to be weakly correlated (with a correlation coefficient of 0.22, see Figure 16). In fact, the OBC galaxy with the reddest $B - V$ has the second most blue $O - E$ color! This discrepancy between $O - E$ and $B - V$ colors for OBC galaxies is especially startling when compared to the behavior of galaxies in the RC3 galaxies

which show a significant correlation between $O - E$ and $B - V$ colors. For 618 RC3 galaxies with B and V color information cross-identified with the APS catalog (see the “photometry” column of Table 4), we find a correlation coefficient of 0.68 between APS $O - E$ and RC3 $B - V$ colors. The radically different photometric behavior of the LSBs from OBC and the HSB galaxies in the RC3 can be understood if we consider the blue and red bandpass behavior separately.

We expect that the blue O and B magnitudes of galaxies should be correlated because the O bandpass covers the entire B bandpass and extends a bit blueward. For the 617 higher surface brightness RC3 galaxies with both B and O measurements available reveals a strong correlation with a correlation coefficient of $r = 0.90$. In contrast to the overlapping blue bandpasses, the E bandpass lies about 1300Å redward of V , centered near the $H\alpha$ line at 6562Å. Consequently, any correlation between the V and E magnitudes might be expected to be weaker. However, we find that E and V magnitudes for the RC3 are only slightly less well correlated ($r = 0.88$) than the O and B bandpasses. What is surprising is that similar investigation of the OBC galaxies shows much weaker correlations between O and B ($r = 0.66$) and E and V ($r = 0.61$). A direct comparison of the two samples shows that if we fit the relationship for RC3 galaxies B versus O magnitudes with a linear fit, the fainter and more diffuse OBC galaxies lie at systematically fainter POSS I O magnitudes than this fit would predict (See Figures 18a). The faintest OBC galaxies appear to have O magnitudes 1 to 2 magnitudes fainter than suggested by their B magnitudes if we extrapolate the RC3 relationship between these two magnitudes. The situation with the E magnitudes is more extreme, with the roughly half of OBC galaxies appearing to be 2 to 3 magnitudes fainter in E than predicted based an extrapolation of the RC3 relationship between E and V 18b). It is the difference in these two effects that results in the OBC galaxies having $O - E$ colors considerably bluer than their $B - V$ colors would suggest (Figure 18c).

7.2. An Explanation for the “Blue Edge”

Since the whole field of LSBs was opened up by Disney’s realization that surface brightness was being generally ignored as a selection effect (Disney 1976), let us consider the possibility that the “blue edge” effect is due to the surface brightness limits of the POSS I plates. The APS Catalog is constructed from digital scans of the POSS I performed in threshold densitometry mode where data is kept only for regions with photographic densities greater than 65% the sky density, resulting in a threshold surface brightness limit for objects in the APS catalog slightly deeper than the sky surface brightness on each plate (See Table 1). It has been established by the APS Project that the limiting surface brightness, $\mu(lim)$, of the POSS I O (blue) plates is typically deeper than that of the E (red) plates. This is not an issue when comparing high surface brightness galaxy photometry where the majority of the galaxy’s luminosity comes from HSB regions. However, it is possible for a LSB galaxy with neutral color and mean surface brightness near the plate limit to barely appear on the E plate while clearly appearing on the O plate due to the deeper surface brightness

limits. This will result in a reported bluer $O - E$ than an otherwise similar HSB galaxy.⁷ This suggests that LSBs may be biased to lie on the “blue edge” of POSS I color-magnitude parameter space simply as a result of the fact that $\mu_E(lim) < \mu_O(lim)$ and not necessarily because they are intrinsically blue.

To support this theory, we investigated the differences between the O and B (and E and V) magnitudes for the OBC galaxies versus $\mu_B(0)$, their reported B central surface brightness (see Figures 19a and 19b). In Figure 19a we see that the difference between the O and B magnitudes is mildly affected by the $\mu_B(0)$ of the OBC galaxy, with a computed best-fit line of the form

$$O - B = -7.874(\pm 3.901) + 0.383(\pm 0.171)\mu_B(0). \quad (5)$$

Figure 19b shows the corresponding relationship for $E - V$ is considerably stronger with

$$E - V = -21.281(\pm 6.079) + 0.984(\pm 0.266)\mu_B(0). \quad (6)$$

The fact that the relationship between these magnitude differences and central surface brightness is steeper for the redder bandpasses (E and V) is simply a reflection of the fact that $\mu_E(lim) < \mu_O(lim)$. The net result is that the $O - E$ colors of LSBs are systematically bluer on the POSS I than they would be on a survey achieving equal surface brightness limits in both red and blue bandpasses.

In passing, we note that the POSS I blue plates (with their deeper surface brightness limits) appear to have a very linear relationship between B and O up to $B \sim 18.5$ (Figure 18a), meaning our estimates of the gas mass-to-light ratios of our “blue edge” galaxies should not be strongly affected by this problem. However, any future attempts to probe for LSBs close to the plate limit may have to compensate for this bias in the O magnitudes of low surface brightness objects near the plate limit.

7.3. Red LSBs on the POSS I

Given this systematic bias for LSBs to appear blue on the POSS I, what can we say about known LSBs that are observed to be red in $O - E$? Returning to Figure 8 we notice that there is a substantial population of LSBs that have colors significantly redward of the “blue edge” boundary (defined in equation 1). An investigation of these very red LSBs shows they in truth are red. First of all, while in almost all cases the mean O (blue) surface brightnesses of these galaxies are lower than their mean E (red) surface brightnesses, red galaxies exhibit larger differences between the blue and red surface brightnesses just as one would expect (see Figure 17a). Furthermore, if the galaxies are truly red, then we would expect their O plate images to be smaller than their E plate

⁷In fact, this represents a previously known selection effect, since extremely blue low surface brightness objects will not appear on the E plate at all, and thus will not reside in the APS catalog.

images. Despite the fact that the E plates usually have shallower surface brightness limits than the O plates, we confirm that the O plate images for the red LSBs are smaller than the E plate images (see Figure 17b). These two facts together imply that these red galaxies are indeed red LSBs.

8. Conclusions

We have developed a simple criterion for identifying HI-rich galaxy candidates from the POSS I based on their positions in POSS I bivariate color-magnitude parameter space. While the method described here relies on followup visual inspection of candidates to eliminate star-galaxy and star-star blended images, subsequent investigation of the image parameters of the “rejected” shows they consist mainly of images with higher surface brightnesses and smaller second moments, suggesting automation of our selection method is possible. Such automation should allow us to identify fainter and smaller “blue edge” candidates than is practical with visual inspection. We observed 31 of our 71 “blue edge” candidates and detected 19 (61%) in HI (15 with high signal-to-noise).

The “blue edge” galaxies we detect in HI are very distinct from “normal” HSB galaxies in both their optical and HI properties. We have concluded that our “blue edge” galaxies are very similar to LSBs in these properties, based on cross-identification of known LSBs with the POSS I. The evidence supporting this tentative identification of “blue edge” galaxies as LSBs includes several key points:

1. Cross-identification of known LSBs with the POSS I shows that over 68% of them lie blueward of the “blue edge” boundary (defined in equation 1). While this certainly doesn’t mean “blue edge” galaxies need be LSBs, it suggests that many LSBs lie on the “blue edge” of POSS I color-magnitude parameter space.
2. The bivariate brightness distributions of known LSBs and our “blue edge” galaxies are similar, with both populations lying at lower mean surface brightness than HSBs drawn from the ZCAT (Figure 11).
3. The HI masses of “blue edge” galaxies are typically lower and their gas mass-to-light ratios higher than those of luminous HSB galaxies (drawn from the RC3). We find that their gas masses are very similar to those of LSBs at the same redshift, although their gas-mass-to-light ratios do not extend to the highest values seen for LSBs. If we take into account the relationship between $O - E$ color and M_{HI}/L_O seen in Figure 14, we see that blue galaxies appear to have a more limited range of gas mass-to-light ratios than redder galaxies, and blue LSBs exhibit a similar range of M_{HI}/L_O as our “blue edge” galaxies.
4. The two-horned profiles seen for many of our “blue edge” galaxies are typical of galaxies with flat rotation curves. Such flat rotation curves are generally associated with large spirals and LSBs (Verheijen and Sancisi 2001). This combined with their typical HI mass of $\log(M_{\text{HI}}) \sim 9.4$ suggests these are not dwarf galaxies, but rather disk systems.

Based on these pieces of evidence, we believe these “blue edge” galaxies are likely to be LSBs on the high surface brightness end of that population (so as to be visible on the POSS I). They are likely to be disk systems and not the smaller dwarf galaxies commonly associated with LSBs. This suggests our “blue edge” criteria selects the same type of galaxies a blind radio survey (Dickey 1997) or wide-field optical survey (Impey and Bothun 1997; O’Neil *et al.* 1997a) for HI-rich LSBs would select.

While it has been noted that LSBs are among the bluest (non-starbursting) galaxies known (Impey and Bothun 1997), this alone does not appear to be the explanation for why LSBs lie preferentially on the “blue edge” of the POSS I color-magnitude diagram. Specifically, it cannot explain why the “red” (in $B - V$) LSBs from O’Neil *et al.* (1997a) can be blue in $O - E$ (Figure 9). We demonstrate that this is most likely the result of differing surface brightness limits on the POSS I O (blue) versus E (red) plates, which make low surface brightness galaxies appear systematically bluer. This does not mean LSBs are not truly “blue,” it simply means that when working near the limiting surface brightness of a survey, the integrated fluxes must be measured to equal isophotes in all bandpasses in order to assure the colors are not systematically biased. This bias for low surface brightness objects to appear blue on the POSS I means that the “blue edge” is an excellent filter for sifting out LSBs and similar objects from the large number of galaxies in the field.

This model for why LSBs lie on the “blue edge” of the POSS I leads to an important question” just what regions of these LSBs are detected on the POSS I plates? Answering this question will require detailed comparison of POSS I images with deep CCD images. The POSS I most likely only detects the highest surface brightness regions of any LSB. This leads to another interpretation of our “blue edge” galaxies: they could be in a class with NGC 2915, a galaxy which has been identified as a blue compact dwarf but has the HI properties of a “dark” spiral galaxy (Meurer *et al.* 1996). Only observations of blue compact dwarfs deeper than the POSS I plate limits can reveal if they have extremely low surface brightness disks surrounding the detected POSS I images, presumably current star forming regions in an otherwise extremely low surface brightness galaxy.

Finally, we see no simple mechanism to make low surface brightness galaxies appear systematically redder on the POSS I versus CCD observations. We have shown that known LSBs with red $O - E$ colors tend to appear smaller on the O plate and have lower O mean surface brightnesses than blue LSBs (Figure 17), indicating that these galaxies are indeed red. Employing simulations of the ISM of LSBs, Gerritsen and de Blok (1999) were able to reproduce the optical properties of LSBs only when assuming LSBs have a sporadic star formation rate. de Blok’s simulations suggest that roughly 80% of LSBs have some current star formation with young, luminous stars dominating the luminosity and leading to their observed blue colors. The remaining quiescent LSBs should appear red ($B - V > 1$ or approximately $O - E > 0.7$) as they would only have an older stellar population. And while we know the POSS I colors of LSBs are biased to be systematically blue, an examination of Figure 9 shows that approximately 50% of all POSS I galaxies have $O - E > 0.7$, while only $\sim 10\%$ of LSBs on the POSS I do. These redder LSBs could be currently in a quiescent stage in their evolution and as such represent interesting candidates for followup if we want to

search for LSBs with old stellar populations as predicted by Gerritsen and de Blok (1999).

We would like to thank Roberta Humphreys and Evan Skillman for discussions of potential astrophysical causes for the “blue edge.” Thanks to Steve Odewahn for an illuminating conversation on observational systematics in the POSS I and to the anonymous referee for his or her helpful suggestions. JEC thanks the Department of Physics, Astronomy, and Engineering Science at Saint Cloud State University who provided him with support when some of this research was conducted and Bruce Partridge for reviewing a late draft of this paper.

We express our gratitude to Karen O’Neil and Jo Ann Eder for providing electronic versions of the data from their respective low surface brightness galaxy catalogs.

We would like to thank telescope operators Miguel Boggiano, Willie Portalatin, Pedro Torres, and Norberto Despiau for their good humor and help with observing (and especially Norberto for his “lucky coffee”). JEC would like to thank Chris Salter, Tapasi Ghosh, Jo Ann Eder, and Phil Perillat for helping make his first radio observing experience excellent, both professionally and personally. Travel was sponsored by the National Astronomy and Ionosphere Center (NAIC) and the University of Minnesota Graduate School.

This research was financially supported by the University of Minnesota and NSF grants AST 97-32695 and AST 00-71192. This research has made use of the APS Catalog of the POSS I, which is supported by the National Aeronautics and Space Administration and the University of Minnesota. The APS databases can be accessed at <http://aps.umn.edu/> on the World Wide Web.

We acknowledge the use of NASA’s *SkyView* facility (<http://skyview.gsfc.nasa.gov>) located at NASA Goddard Space Flight Center.

REFERENCES

Briggs, F.H. 1997, ApJ, 484, 618

Burstein, D. and Heiles, C. 1982, AJ, 87, 1165

Bothun, G.D. 1982, ApJS, 50, 39

Bothun, G.D. 1984, ApJ, 277, 532

Bothun, G.D., Impey, C.D., Malin, D.F., & Mould, J.R. 1987, AJ, 94, 23

Bothun, G.D., Impey, C., and McGaugh, S. 1997, PASP, 109, 745

Cabanela, J.E., and Aldering, G. 1998, AJ, 116, 1094

Cabanela, J.E., and Dickey, J.M. 1999, AJ, 118, 46

Cardelli, J. A., Clayton, G. C, and Mathis, J. S. 1989, *ApJ*, 345, 245

Cayatte, V., Kotanyi, C., Balkowski, C., & van Gorkom, J.H. 1994, *AJ*, 107, 1003

de Blok, W.J.G., McGaugh, S.S., and van der Hulst, J.M. 1996, *MNRAS*, 283, 18

de Vaucouleurs, G., de Vaucouleurs, A., Corwin, H.G. Jr., Buta, R.J., Paturel, G., and Fouqué, P. 1991, *Third Reference Catalogue of Bright Galaxies* (Springer-Verlag, New York)

Dickey, J.M. 1997, *AJ*, 113, 1939

Disney, M.J. 1976, *Nature*, 263, 573

Dressler, A. 1980, *ApJ*, 236, 351

Driver, S. and Cross, N. 2000, in *Mapping the Hidden Universe (ASP Conference Series Vol. 218)*, (Astronomical Society of the Pacific, San Francisco), 309.

Eder, J., Oemler, A.J., Schombert, J.M. and Dekel, A. 1989, *ApJ*, 340, 29

Eder, J.A. and Schombert, J.M. 2000, [astro-ph/0006290](#)

Giovanelli, R. and Haynes, M.P. 1985, *ApJ*, 292, 404

Giovanelli, R., Haynes, M.P., and Chincarini, G.L. 1986, *ApJ*, 300, 77

Giovanelli, R. and Haynes, M.P. 1988, in *Large-Scale Structures of the Universe, IAU Symp. 130*, (Kluwer Academic Publishers, Dordrecht), 113

Giraud, E. 1987, *A&A*, 178, 310

Gerritsen, J.P.E. and de Blok, W.J.G. 1999, *A&A*, 342, 655

Huchra, J., Geller, M., Clemens, C., Tokarz, S and Michel, A. 1992, *Bull. C.D.S.* 41, 31. (ZCAT, February 2000 version)

Impey, C.D., Sprayberry, D., Irwin, M.J., and Bothun, G.D. 1996, *ApJS*, 105, 209

Impey, C. and Bothun, G.D. 1997, *ARA&A*, 35, 267

Lasker, B.M., Sturch, C.R., McLean, B.J., Russell, J.L., Jenkner, H., & Shara, M.M. 1990, *AJ*, 99, 2019

Lavezzi, T.E. and Dickey, J.M. 1997, *AJ*, 114, 2437

Maia, M.A.G., Willmer, C.N.A., and Da Costa, L.N. 1998, *AJ*, 115, 49

Martin, C.L. and Kennicutt, R.C. 2001, *ApJ*, 555, 301

Matthews, L.D. and Gallagher, J.S. 1997, *AJ*, 114, 1899

Meurer, G.R., Carignan, C., Beaulieu, S.F., and Freeman, K.C. 1996, AJ, 111, 1551

Nilson, P. 1974, Uppsala Astron. Obs. Annals, 6 (The Uppsala General Catalog of Galaxies, UGC)

Odewahn, S.C., Stockwell, E.B., Pennington, R.L., Humphreys, R.M., and Zumach, W.A. 1992, AJ, 103, 318

O'Neil, K., Bothun, G.D., and Cornell, M. 1997, AJ, 113, 1212 (OBC)

O'Neil, K., Bothun, G.D., Schombert, J., Cornell, M., and Impey, C.D. 1997, AJ, 114, 2448

O'Neil, K., Bothun, G.D., and Schombert, J. 2000, AJ, 119, 136

Pennington, R.L., Humphreys, R.M., Odewahn, S.C., Zumach, W., Thurmes, P.M. 1993, PASP, 105, 521

Pildis, R.A., Schombert, J.M., and Eder, J.A. 1997, ApJ, 481, 157

Press, W.H., Teukolsky, S.A., Vetterlin, W.T., and Flannery, B.P. 1992, *Numerical Recipes in C (Second Edition)* (Cambridge University Press, New York), 627

Roberts, M.S. and Haynes, M.P. 1993, ARA&A, 32, 115

Romanishin, W., Strom, K.M., and Strom, S.E. 1983, ApJS, 52, 105

Salzer, J.J. and Norton, S.A. 1999, in *The Low Surface Brightness Universe (ASP Conference Series Vol. 170)*, (Astronomical Society of the Pacific, San Francisco), 253.

Schlegel, D., Finkbeiner, D.P., and Davis, M. 1998, AJ, 500, 525

Schneider, S.E., Thuan, T.X., Magri, C. and Wadiak, J.E. 1990, ApJS, 72, 245

Schneider, S.E., 1996, in *The Minnesota Lectures on Extragalactic Neutral Hydrogen (ASP Conference Series 106)* (Astronomical Society of the Pacific, San Francisco), 323

Schombert, J.M., Bothun, G.D., Schneider, S.E., and McGaugh, S.S. 1992, AJ, 103, 1107

Schombert, J.M., Pildis, R.A., and Eder, J.A. 1997, ApJS, 111, 223

Shane, C. D., and Wirtanen, C. A. 1967, Publ. Lick. Obs. 22, part 1

Skillman, E.D., 1996, in *The Minnesota Lectures on Extragalactic Neutral Hydrogen (ASP Conference Series 106)* (Astronomical Society of the Pacific, San Francisco), 208

Sprayberry, D., Impey, C.D., and Irwin, M.J. 1996, ApJ, 463, 535.

Stavely-Smith, L., Davies, R.D., and Kinman, T.D. 1992, MNRAS, 258, 334

Staveley-Smith, L., Marquarding, M., Kilborn, V.A., & Webster, R.L. 2001, *Gas and Galaxy Evolution (ASP Conference Proceedings, Vol. 240)*, (Astronomical Society of the Pacific, San Francisco), 427

Taylor, C.L. Thomas,D.L., Brinks, E., Skillman, E.D. 1996, ApJS, 107, 143

Theureau,G., Bottinelli,L., Coudreau-Durand,N., Gouguenheim,L., Hallet,N., Loulergue,M., Paturel,G., Teerikorpi,P. 1998, A&AS, 130, 333

van der Hulst, J.M., Skillman, E.D., Smith, T.R., Bothun, G.D., McGaugh, S.S., & de Blok, W.J.G. 1993, AJ, 106, 548

van Zee, L. 1999, in *The Low Surface Brightness Universe (ASP Conference Series Vol. 170)*, (Astronomical Society of the Pacific, San Francisco), 274.

Verheijen, M.A.W. and Sancisi, R. 2001, A&A, 370, 765

Wegner,G., Haynes, M.P., Giovanelli, R. 1993, AJ, 105, 1251

Weinberg, S. 1972, *Gravitation and Cosmology* (New York:Wiley)

Fig. 1.— A POSS I color-magnitude diagram of galaxies in the Hercules cluster from the four fields in Dickey (1997). Notice that the vast majority of these HI-rich galaxies lie on the “blue edge” of the color-magnitude diagram. Note: An approximate color transformation for $O - E$ to more contemporary bandpasses is $O - E \approx B - R + 0.30$ as noted by Cabanela and Aldering (1998).

Fig. 2.— The final histogram of the total fraction of observing time which was flagged due to radio frequency interference versus frequency. The top (bottom) panel shows right (left) circular polarization.

Fig. 3.— HI spectra and 3' by 3' POSS I (Red) images of candidates detected in HI including NGC 634. Segments of the spectral profile determined to be due to interference are blanked.

Fig. 4.— The four HI spectra and POSS I (Red) image of the region surrounding MAPS-P295-1369071, where there was the possibility of confusion with NPM1G +30.0027. As before, segments of the spectral profile determined to be due to interference are blanked.

Fig. 5.— Like Figure 3, but for galaxies tentatively detected in HI.

Fig. 6.— Like Figure 3, but for candidates detected in HI in the off scans. Images are of the off scan positions in each case.

Fig. 7.— (a) A plot of the logarithm of the HI mass (in units of solar mass) versus the angular distance (in degrees) from the PPS ridgeline (Cabanela and Aldering 1998) for the “blue edge” galaxies. All objects which were undetected are shown as downward arrows indicating the estimated upper HI mass limit for the observed “blue edge” galaxies not detected in HI. (b) A plot of M_{HI}/L_O versus the angular distance from the PPS ridgeline for the “blue edge” galaxies. The best fit line is shown and is described by equation 3. This best fit line reflects a weak correlation ($r = 0.255$) between M_{HI}/L_O and distance from the PPS ridgeline.

Fig. 8.— The POSS I color-magnitude distribution of the APS Catalog galaxies versus those of the HI-rich and LSB galaxies in Dickey (1997), O’Neil *et al.* (1997a), Schombert *et al.* (1997), Romanishin, Strom, & Strom (1983), and Impey *et al.* (1996). Most of the HI-rich and LSB galaxies lie blueward the “blue edge” boundary defined by the bluest 10% of APS Catalog galaxies.

Fig. 9.— The cumulative $\Delta(O - E)_{BE}$ distributions for APS galaxies and various HI-rich and LSB galaxy catalogs. While (by definition) only 10% of APS galaxies lie blueward of the “blue edge,” well over 60% of the HI-rich and LSB galaxies lie blueward of the “blue edge.”

Fig. 10.— The “Bivariate Brightness Distribution” (BBD) for our observed “blue edge” galaxies versus the ZCAT. Notice that the “blue edge” population appears to be fainter and of lower surface brightness than the ZCAT population (labeled with dots). The separation in luminosity is expected given the flux-limits of the ZCAT, but distinction in surface brightness between the two populations hints that our “blue edge” galaxies are a distinct galaxy population from those in the ZCAT.

Fig. 11.— A BBD plot like Figure 10 but adding the O’Neil *et al.* (1997a) and Impey *et al.* (1996) LSB catalogs. Our “blue edge” galaxies (labeled with crosses) lie among the LSB catalog galaxies.

Fig. 12.— (a) A plot of distribution of $M_{H\text{I}}$ values in 4 galaxy catalogs with an imposed flux limit of $m_E < 20$ and redshift range of $4000 \text{ km s}^{-1} < cz < 9000 \text{ km s}^{-1}$. The distributions are all scaled to the total number of galaxies in the sample, with fractional counts computed in bins of 0.33 dex in $M_{H\text{I}}$. (b) A plot of distribution of $M_{H\text{I}}/L_O$ values for the same galaxy catalogs as in (a) computed for bin widths of 0.30 dex in $M_{H\text{I}}/L_O$.

Fig. 13.— A plot of $M_{H\text{I}}$ versus L_O (in solar units) for the “blue edge” galaxies and other galaxy catalogs mentioned in text, where $4000 \text{ km s}^{-1} < cz < 9000 \text{ km s}^{-1}$ and $E < 20$. The imposed flux limit of $m_E < 20$ corresponds to a limiting luminosity of $\log(L_O) \gtrsim 7.7$ in solar units, roughly the luminosity of the dimmest LSBs on this plot but considerably dimmer than the least luminous “blue edge” galaxy.

Fig. 14.— A plot of $M_{H\text{I}}/L_O$ (in solar units) versus O-E color for the “blue edge” galaxies, the HSB galaxies from the RC3, and LSB galaxies from Impey *et al.* (1996) and O’Neil *et al.* (1997a). Whereas the bluest galaxies only range over ~ 0.6 dex in $M_{H\text{I}}/L_O$, the reddest galaxies range over 3 orders of magnitude in $M_{H\text{I}}/L_O$, reaching gas mass-to-light ratios an order of magnitude higher than those seen for the bluest galaxies.

Fig. 15.— (a) B_{tot} vs. $B - V$ color-magnitude diagrams for the OBC for galaxies matched or unmatched to the APS Catalog. (b) Histograms of the B central surface brightnesses of OBC galaxies (uncorrected for galaxy inclination) separated by whether the data is matched or unmatched to the APS Catalog. There is evidence of the expected bias against selecting the extremely low surface brightness objects from the OBC.

Fig. 16.— A plot of $B - V$ color (from OBC) versus $O - E$ color (from the APS Catalog of the POSS I) for cross-identified OBC galaxies. The two colors appear to be very weakly correlated.

Fig. 17.— Plots of the $O - E$ colors for galaxies in Impey *et al.* (1996), O’Neil *et al.* (1997a), and this study versus (a) the difference in O and E surface brightness and (b) the difference in O and E image surface area.

Fig. 18.— Plots comparing the measured fluxes of RC3 versus OBC galaxies. (a) A plot of POSS I O magnitude versus B magnitudes for both the RC3 and OBC. The best fit linear relationship for O vs B , derived for the RC3 galaxies alone, is shown. The faintest OBC galaxies all lie above the best fit line, suggesting their POSS I O magnitudes are all fainter than the RC3-based relationship between O and B would suggest. (b) A similar plot to (a) except for POSS I E versus V magnitudes. In this case, the vast majority of the OBC galaxies lie at fainter POSS I E magnitudes than the RC3-based relationship would suggest. (c) The combination of the two effects illustrated in (a) and (b) is that the OBC galaxies have systematically bluer POSS I $O - E$ colors than their RC3 counterparts for

comparable $B - V$ colors.

Fig. 19.— (a) The difference of POSS I O magnitude and B magnitudes for OBC galaxies versus their central surface brightness ($\mu_B(0)$) from OBC). The best fit line to this data has a slope of 0.383 ± 0.171 , indicating a weak trend in $O - B$ versus $\mu_B(0)$. (b) A similar plot to (a) except for the difference in POSS I E and V magnitudes versus $\mu_B(0)$. The effect is more dramatic in this case, with the best-fit line on this plot having a slope of 0.984 ± 0.266 . (c) The two effects illustrated in (a) and (b) combine such that the difference between $O - E$ and $B - V$ colors for OBC will become larger (with bluer $O - E$ than $B - V$ values) as we move toward more diffuse $\mu_B(0)$ values.

Table 1. POSS I Plate Parameters from the APS Catalog for POSS I Fields in this Study

Field Number	Field Center		$\mu_{threshold}$	
	α (B1950)	δ (B1950)	O	E
P293	00:04:53.00	+30:31:45.00	23.8	23.6
P294	00:31:01.00	+30:31:31.00	24.6	23.1
P295	00:57:11.00	+30:30:46.00	23.7	23.0
P296	01:23:30.00	+30:28:12.00	24.6	22.6
P297	01:49:25.00	+30:28:25.00	23.9	22.9
P445	16:04:17.00	+17:44:28.00	23.7	23.2

Table 2. HI-rich Candidates List

Object	α (B1950)	δ (B1950)	E ^a	O-E ^a	E(B-V) ^b	Date ^c	Comments ^d
MAPS-P293-137994	23:51:14.72	+30:55:51.42	18.02	-0.69	0.079	11	Non-Detection
MAPS-P293-268610	00:02:39.36	+28:36:23.43	18.74	-0.21	0.052	08 & 09	Off Beam on UGC 105 (8th)
MAPS-P293-100987	00:04:52.45	+31:47:35.03	17.76	-0.59	0.040	16	EOSD F409-05 (On Beam) Off Beam Detection
MAPS-P293-211328	00:09:59.12	+29:40:06.63	19.19	-0.84	0.054
MAPS-P293-249588	00:11:59.58	+29:07:58.17	18.45	-0.31	0.041
MAPS-P293-249758	00:12:36.01	+28:58:22.68	19.20	-0.46	0.035	10 & 11	Strong RFI(10 th) Narrow RFI(11 th)
MAPS-P293-179271	00:13:36.89	+30:13:54.80	18.28	-0.33	0.064	20	...
MAPS-P293-180077	00:16:18.49	+30:14:11.05	16.79	-0.01	0.075	...	SRGb062.66
MAPS-P293-239452	00:18:11.89	+29:08:00.91	17.95	-0.18	0.035
MAPS-P294-766044	00:30:34.46	+28:07:38.66	18.61	-0.29	0.045	08	Non-Detection
MAPS-P294-241809	00:31:15.32	+31:10:32.02	15.89	0.29	0.056	...	UGC 334
MAPS-P294-727319	00:41:23.79	+28:36:05.96	17.81	-0.35	0.046	16	UGC 467
MAPS-P295-1977899	00:43:43.40	+29:21:04.69	15.90	0.06	0.053	...	CGCG 500-083
MAPS-P295-2259922	00:43:51.97	+28:44:55.64	19.75	-0.99	0.061	10 & 11	Non-Detection Strong RFI(10 th)
MAPS-P295-922471	00:44:49.60	+31:23:00.05	16.06	0.14	0.067	...	CGCG 500-095
MAPS-P295-2526723	00:45:28.88	+28:13:59.64	18.16	-0.32	0.069
MAPS-P295-1880836	00:45:30.18	+29:40:43.94	19.45	-0.75	0.063	15	Non-Detection
MAPS-P295-2261674	00:46:15.89	+28:47:25.55	17.02	-0.14	0.056
MAPS-P295-1031187	00:47:26.93	+31:13:33.74	17.82	-0.22	0.063
MAPS-P295-2078102	00:47:28.05	+29:11:06.88	17.83	-0.20	0.054
MAPS-P295-2262929	00:47:52.74	+28:50:56.86	16.63	-0.14	0.058
MAPS-P295-1577104	00:48:04.78	+30:15:29.53	18.01	-0.34	0.072	12	FGC012A (On Beam) Non-Detection Off Beam Detection
MAPS-P295-1474797	00:49:15.50	+30:26:37.99	18.98	-0.68	0.072	14	Non-Detection
MAPS-P295-585461	00:49:18.24	+32:09:13.14	18.40	-0.22	0.064	08	Non-Detection
MAPS-P295-699736	00:49:56.50	+31:56:30.93	18.42	-0.63	0.068	10 & 11	...
MAPS-P295-1369071	00:50:18.47	+30:44:33.45	18.51	-0.23	0.055	12, 13, 14, & 15	NPM1G +30.0027 in field (see text)
MAPS-P295-487139	00:50:38.45	+32:21:58.70	17.36	-0.23	0.078
MAPS-P295-1790367	00:50:39.52	+29:48:48.71	18.93	-0.54	0.066	08 & 09	Non-Detection
MAPS-P295-2270262	00:51:13.28	+28:50:59.67	16.24	0.12	0.055
MAPS-P295-823940	00:51:56.55	+31:43:18.81	18.43	-0.60	0.061	08 & 09	Non-Detection Strong RFI(8 th)
MAPS-P295-1894424	00:52:47.08	+29:37:56.13	19.20	-0.49	0.065
MAPS-P295-1693362	00:52:49.86	+30:07:37.67	15.87	0.05	0.065	08	CGCG 501-047
MAPS-P295-829092	00:53:34.38	+31:41:46.88	19.03	-0.58	0.063
MAPS-P295-391670	00:54:34.29	+32:35:19.01	17.68	-0.14	0.058
MAPS-P295-392980	00:54:54.66	+32:29:53.83	16.47	-0.37	0.056	...	In MAPS-PP
MAPS-P295-500031	00:55:00.42	+32:16:35.34	15.98	-0.05	0.057	...	CGCG 501-080
MAPS-P295-296064	00:55:38.66	+32:38:37.09	19.35	-0.65	0.057	10	Non-Detection
MAPS-P295-951462	00:56:09.78	+31:28:52.05	18.09	-0.36	0.062
MAPS-P295-1275729	00:56:19.32	+30:53:48.70	17.09	-0.04	0.067
MAPS-P295-1386371	00:57:06.42	+30:42:58.33	18.70	-0.25	0.065
MAPS-P295-83632	00:57:21.92	+33:18:18.40	19.06	-0.51	0.058	13	Some RFI

Table 2—Continued

Object	α (B1950)	δ (B1950)	E ^a	O-E ^a	E(B-V) ^b	Date ^c	Comments ^d
MAPS-P295-1387790	00:57:32.61	+30:43:53.15	18.41	-0.25	0.062
MAPS-P295-2202485	00:57:44.62	+29:03:54.80	19.06	-0.60	0.073
MAPS-P295-1915216	00:58:22.06	+29:40:19.07	18.88	-0.82	0.059	10	UGC 630 in field (see text)
MAPS-P295-1915437	00:58:24.48	+29:39:55.20	19.21	-0.71	0.059
MAPS-P295-1284440	00:58:45.37	+30:55:24.13	16.86	0.03	0.058
MAPS-P295-1067425	00:59:25.98	+31:15:16.14	18.60	-0.20	0.054	10	Non-Detection
MAPS-P295-1069708	00:59:52.52	+31:16:36.26	17.66	-0.33	0.053
MAPS-P295-230677	01:00:24.99	+32:51:30.43	18.49	-0.30	0.059	08 & 17	Non-Detection
MAPS-P295-156408	01:00:38.44	+33:11:53.30	19.79	-0.91	0.066
MAPS-P295-2124445	01:00:59.18	+29:19:21.73	16.81	-0.14	0.063
MAPS-P295-532118	01:01:00.18	+32:16:23.27	18.50	-0.45	0.067	10	Non-Detection
MAPS-P295-1615585	01:01:01.86	+30:18:09.08	18.71	-0.50	0.056	11	Non-Detection
MAPS-P295-325936	01:01:13.58	+32:41:43.41	16.35	-0.38	0.058	...	UGC 657
MAPS-P295-1827388	01:01:38.08	+29:54:52.26	18.61	-0.32	0.067	11	Non-Detection
MAPS-P295-434368	01:01:50.90	+32:30:24.65	19.48	-0.84	0.059
MAPS-P295-642385	01:01:55.27	+32:03:44.94	18.42	-0.25	0.065	08 & 09	...
MAPS-P295-100980	01:03:09.63	+33:15:13.49	16.89	-0.25	0.055	...	In MAPS-PP
MAPS-P295-102863	01:03:38.14	+33:20:16.32	16.01	0.20	0.054	...	KUG 103+333
MAPS-P295-657010	01:04:17.94	+32:07:20.98	16.39	-0.04	0.064	...	UGC 679
MAPS-P295-1202937	01:04:19.57	+31:07:44.99	18.66	-0.42	0.056	15	...
MAPS-P295-345620	01:04:30.12	+32:46:51.56	17.12	-0.10	0.061
MAPS-P295-773634	01:05:02.09	+31:57:13.89	19.54	-0.87	0.057	10	...
MAPS-P295-1326244	01:06:28.46	+30:49:28.58	15.84	0.21	0.064	13	Non-Detection
MAPS-P295-357095	01:07:14.10	+32:38:17.48	16.47	0.07	0.064	...	KUG0107+326A
MAPS-P295-357226	01:07:16.59	+32:39:56.58	17.95	-0.34	0.064	...	In MAPS-PP
MAPS-P295-357773	01:07:25.88	+32:38:05.88	19.19	-0.70	0.061
MAPS-P295-359427	01:07:57.89	+32:45:57.00	16.44	0.13	0.052	...	KUG0107+327
MAPS-P295-362727	01:09:11.75	+32:45:41.71	17.57	-0.15	0.056	...	KUG0107+327A
MAPS-P295-910484	01:09:14.09	+31:41:16.90	17.03	-0.23	0.059	14	Strong RFI
MAPS-P295-576122	01:11:48.60	+32:15:15.97	18.41	-0.32	0.060	10, 11 & 17	...

^aThese values are all corrected for Galactic extinction as described in the text.

^bE(B-V) from Schlegel, Finkbeiner, & Davis (1998).

^cObservation dates (in August 1998) listed if observed. All dates UTC.

^dAll cross-identifications are within 0.5' of known position, and thus falling well within the Arecibo beam. “MAPS-PP” refers to the Minnesota Automated Plate Scanner Pisces-Perseus Catalog of Cabanela and Aldering (1998).

Table 3. HI Observations

Object	F_{obs} (mJy-km s $^{-1}$)	V ^a (km s $^{-1}$)	ΔV (km s $^{-1}$)	Group	$\log M_{HI}$ (M_{\odot})	$\log L$ (L_{\odot})	M_{HI}/L_O (\odot)
MAPS-P293-268610	857.5 (22.3)	8361	151	1	9.44	8.86	3.78
MAPS-P293-100987	1704.0 (23.4)	4851	124	1	9.26	8.77	3.06
MAPS-P293-249758	483.7 (16.4)	6890	116	1	9.02	8.50	3.27
MAPS-P293-179271	508.1 (25.1)	7288	129	1	9.09	8.92	1.47
MAPS-P294-727319	1692.8 (19.2)	4817	137	1	9.25	8.75	3.17
MAPS-P295-699736	1457.5 (14.1)	4899	124	1	9.20	8.52	4.82
MAPS-P295-1790367	628.2 (11.8)	4956	138	1	8.85	8.33	3.31
MAPS-P295-823940	204.2 (10.3)	5362	61	1	8.43	8.59	0.68
MAPS-P295-1693362	1766.3 (21.5)	6667	241	1	9.55	9.81	0.55
MAPS-P295-1915216	389.5 (19.0)	6788	121	1	8.91	8.62	1.95
MAPS-P295-1915216 (UGC 630)	763.7 (16.7)	4878	156	1	8.92	9.71	0.16
MAPS-P295-642385	651.9 (14.6)	4716	94	1	8.82	8.49	2.15
MAPS-P295-1202937	496.1 (10.7)	6280	168	1	8.95	8.64	2.04
MAPS-P295-1326244	279.9 (13.7)	5483	44	1	8.58	9.65	0.09
MAPS-P295-910484	1194.3 (43.9)	6701	170	1	9.39	9.35	1.09
OPSPNT	920.6 (21.5)	5998	170	2
MAPS-P295-1369071	1286.7 (18.3)	5995	175	2	9.32	8.66	4.58
MIDPNT	794.3 (21.9)	5987	162	2
NPM1G +30.0027	311.6 (28.6)	5993	229	2	8.71	10.02	0.05
MAPS-P295-2259922	187.0 (12.9)	5698	129	3	8.44	8.12	2.10
MAPS-P295-83632	436.7 (17.9)	4757	74	3	8.65	8.24	2.59
MAPS-P295-773634	342.0 (28.7)	4918	221	3	8.58	8.08	3.16
MAPS-P295-576122	232.9 (13.9)	6714	135	3	8.68	8.72	0.91
UGC 105	793.6 (28.2)	8065	233	4	> 9.37	10.47	> 0.08
MAPS-P293-102675	1859.8 (24.4)	6570	240	4	> 9.56	9.65	> 0.82
MAPS-P294-444433	290.9 (23.7)	6697	129	4	> 8.77	9.01	> 0.58
NGC 634	4771.5 (38.0)	4928	512	5	9.72	10.49	0.17

^aAll velocities are heliocentric. Comparison between velocities determined using flux density thresholds of 50% the mean flux density and 20% the maximum flux density showed the difference between these two methods to always be less than the uncertainty due to the channel width, therefore we take the uncertainty to be 2 channel widths or 10 km s $^{-1}$ in all cases.

Table 4. Comparison Galaxy Catalogs Used

Source	Number of Catalogs Galaxies used for comparison of...			
	BBD	Color-magnitude	M_{H1}	Photometry
ZCAT (February 2000)	1648	1648	0	0
Dickey (1997)	46	46	0	0
Romanishin, Strom, & Strom (1983)	0	27	0	0
Impey <i>et al.</i> (1996)	343	343	38	0
O'Neil <i>et al.</i> (1997a)	53	53	10	38
Schombert <i>et al.</i> (1997)	0	104	0	0
RC3	0	0	1126	617

Table 5. Estimated Probabilities of Identical Parent $\Delta(O - E)_{BE}$ Distributions

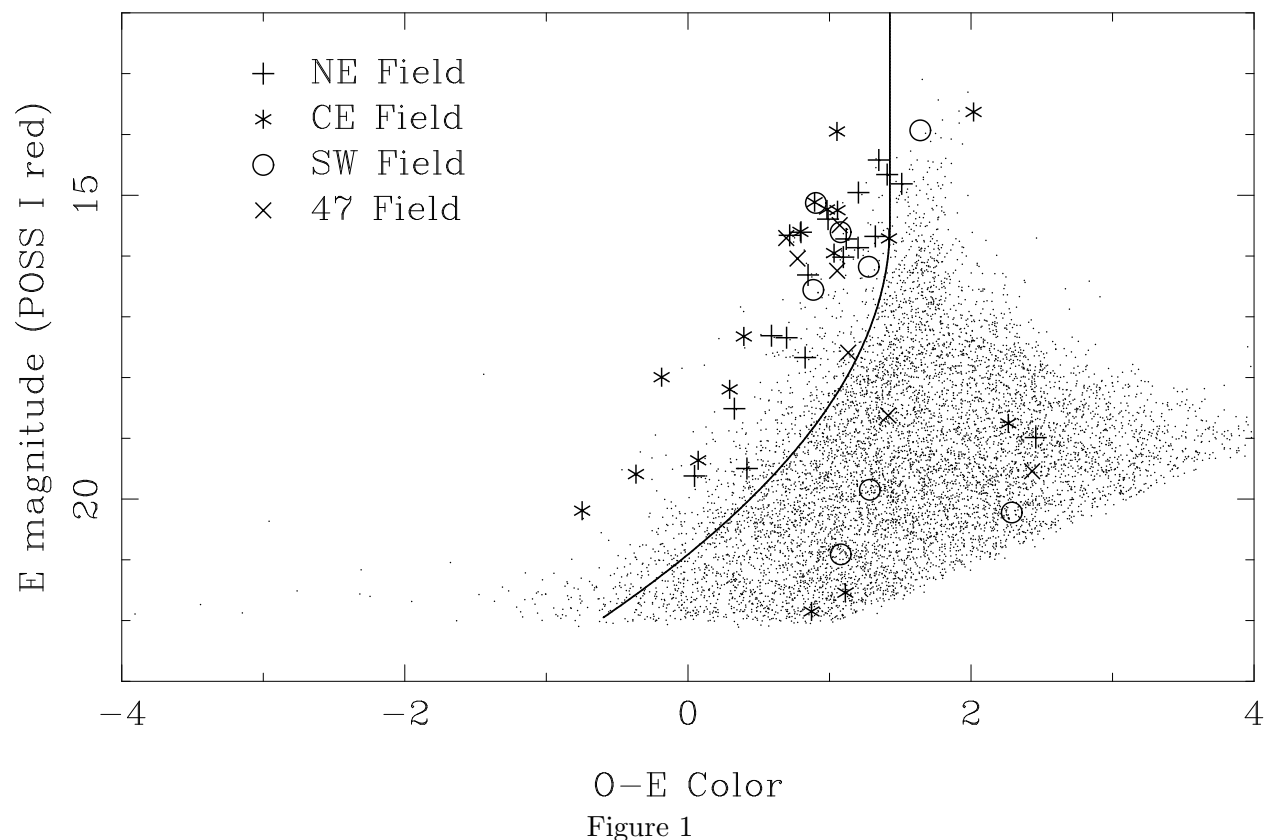
Comparison Sample	Sample Size	log(probability)						
		(1)	(2)	(3)	(4)	(5)	(6)	(7)
(1) APS	7943	0.00	-17.22	-20.56	-16.05	-111.13	-23.88	-34.93
(2) “Blue Edge” Galaxies	19	-17.22	0.00	-12.20	-5.51	-12.63	-7.05	-10.38
(3) Dickey (1997)	51	-20.56	-12.20	0.00	-5.34	-0.64	-2.20	-1.51
(4) Romanishin, Strom, & Strom (1983)	27	-16.05	-5.51	-5.34	0.00	-4.36	-1.18	-2.60
(5) Impey <i>et al.</i> (1996)	347	-111.13	-12.63	-0.64	-4.36	0.00	-1.33	-0.53
(6) O'Neil <i>et al.</i> (1997a)	52	-23.88	-7.05	-2.20	-1.18	-1.33	0.00	-0.39
(7) Schombert <i>et al.</i> (1997)	103	-34.93	-10.38	-1.51	-2.60	-0.53	-0.39	0.00

Table 6. Estimated Probabilities of Identical Parent $M_{H\text{I}}$ Distributions

Comparison Sample	Sample Size	log(probability)			
		(1)	(2)	(3)	(4)
(1) “Blue Edge” Galaxies	19	0.00	-1.10	-0.06	-9.50
(2) Impey <i>et al.</i> (1996)	38	-1.10	0.00	-0.93	-12.23
(3) O’Neil <i>et al.</i> (1997a)	10	-0.06	-0.93	0.00	-5.40
(4) RC3	1126	-9.50	-12.23	-5.40	0.00

Table 7. Estimated Probabilities of Identical Parent $M_{H\text{I}}/L_O$ Distributions

Comparison Sample	Sample Size	log(probability)			
		(1)	(2)	(3)	(4)
(1) “Blue Edge” Galaxies	19	0.00	-0.70	-0.27	-2.53
(2) Impey <i>et al.</i> (1996)	38	-0.70	0.00	-0.12	-4.10
(3) O’Neil <i>et al.</i> (1997a)	10	-0.27	-0.12	0.00	-2.55
(4) RC3	1126	-2.53	-4.10	-2.55	0.00



O-E Color
Figure 1

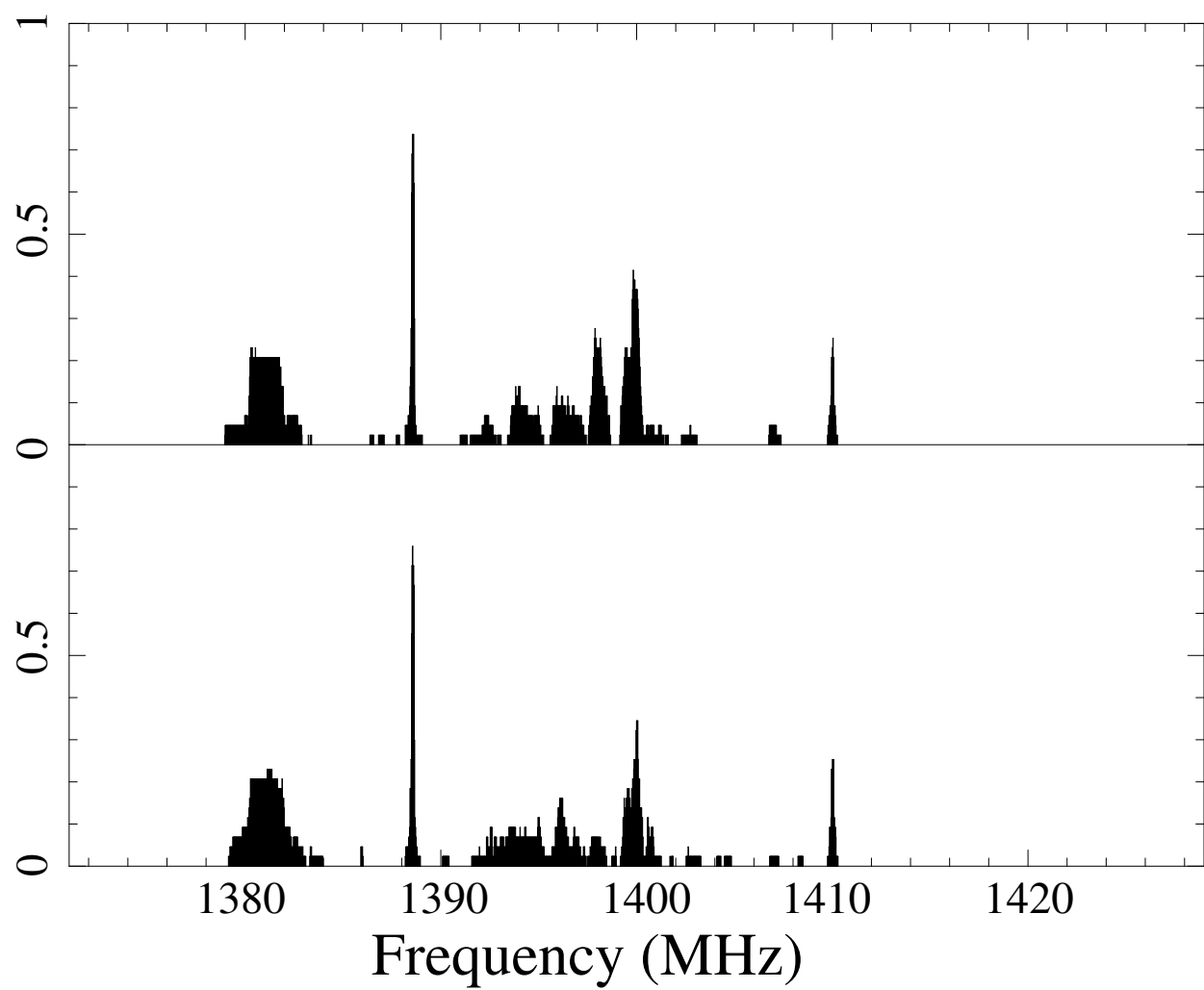


Figure 2

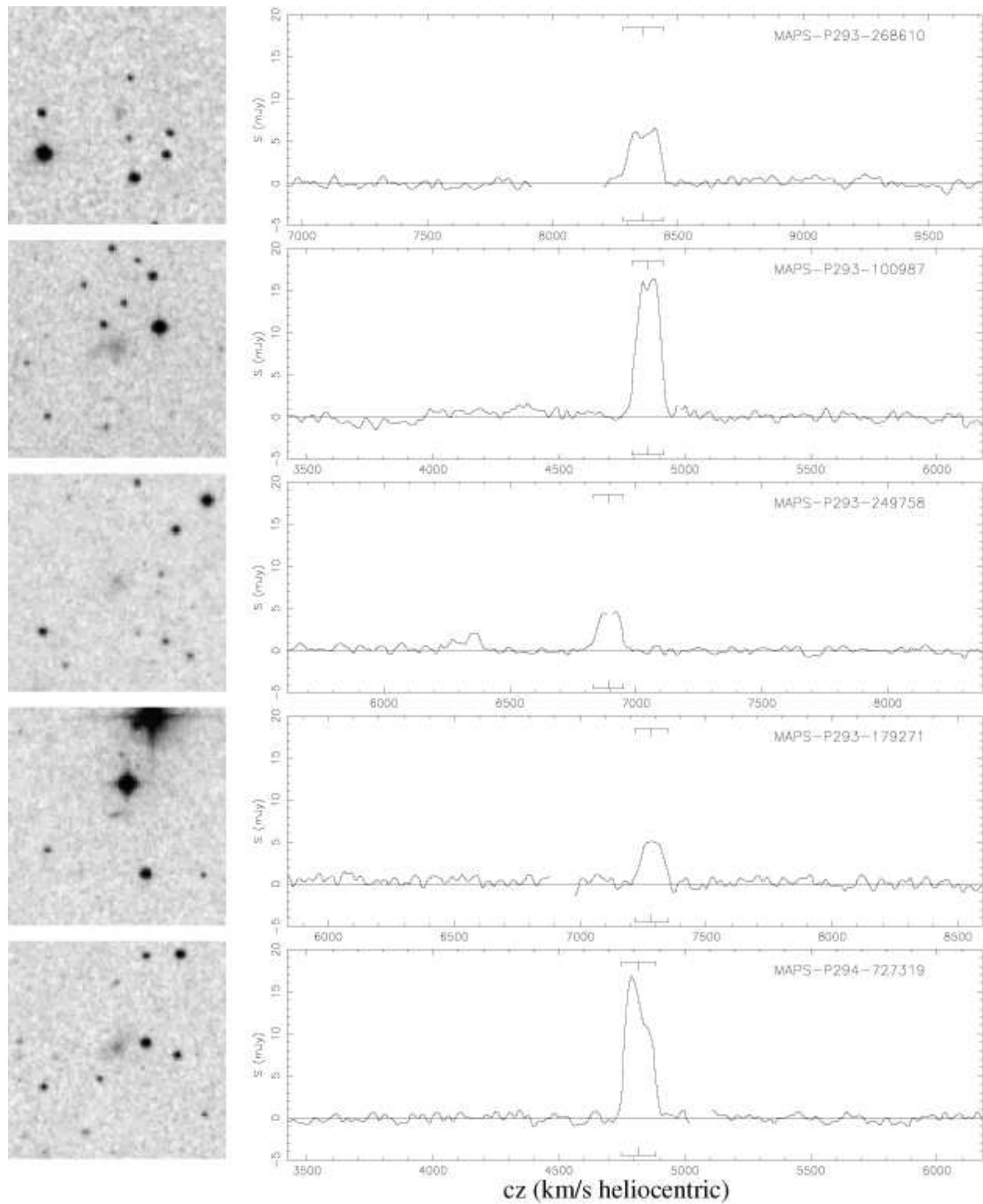


Figure 3

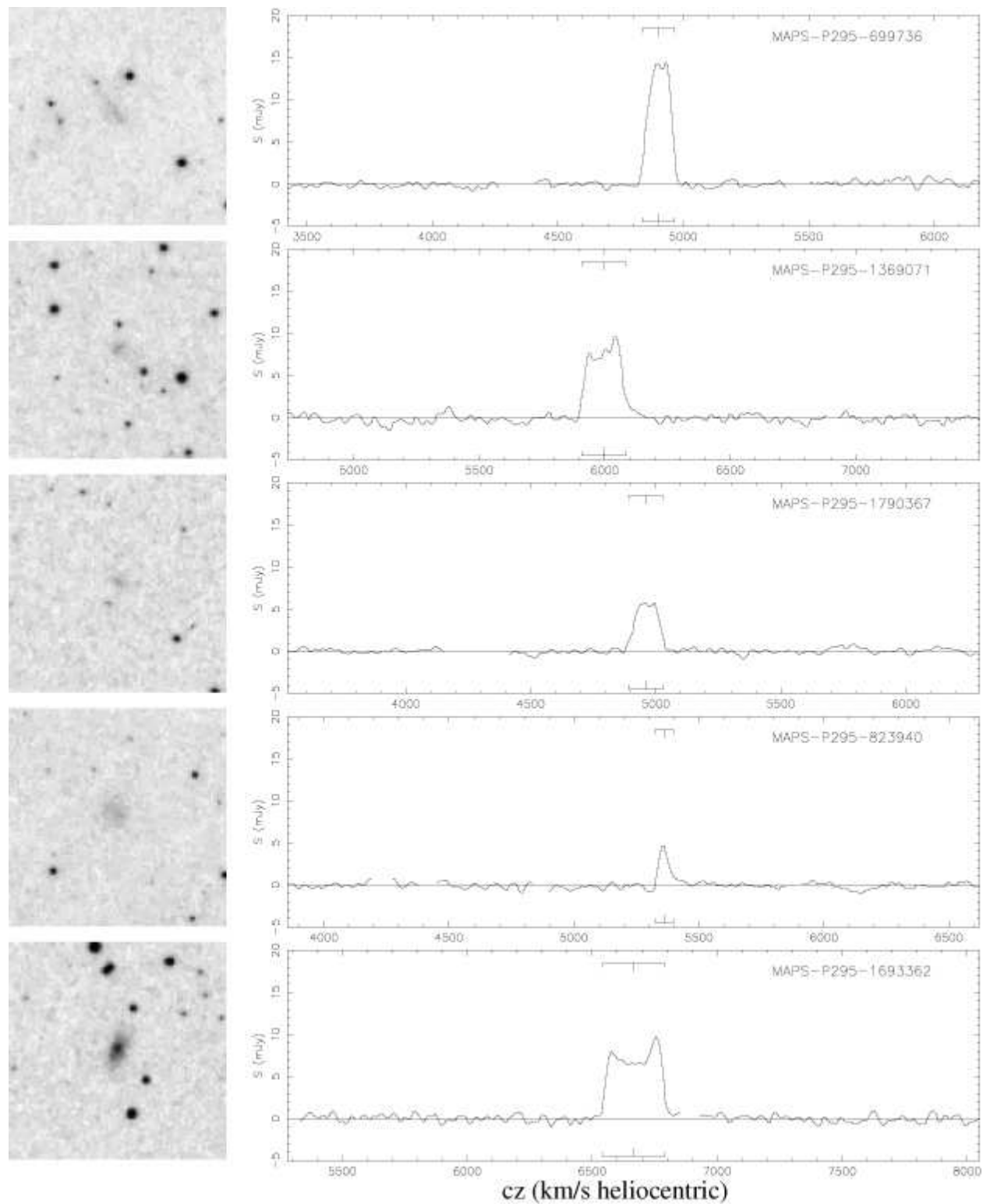
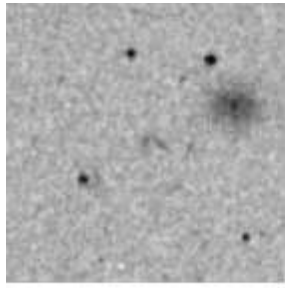


Figure 3 (Continued)



NOTE: UGC 630 is in the center right of this field and has a systemic velocity of 4884 km/s. MAPS-P295-1915216 is the spectra to right.

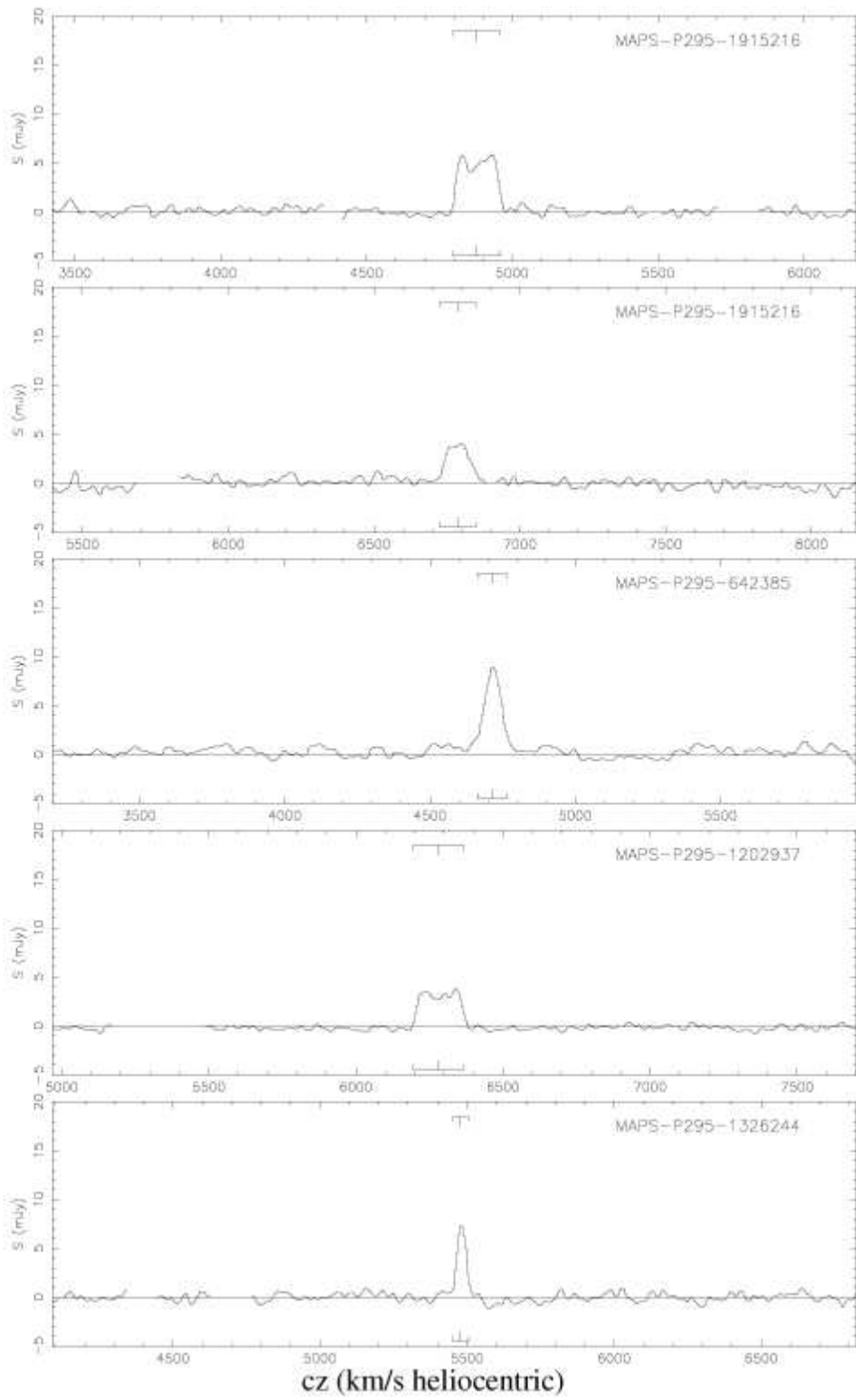
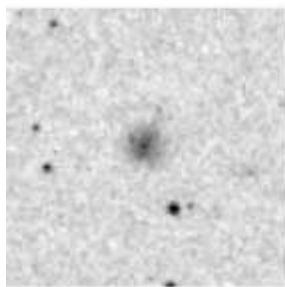
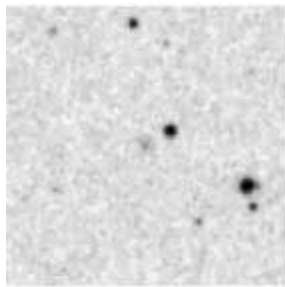
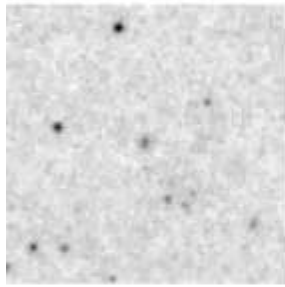


Figure 3 (Continued)

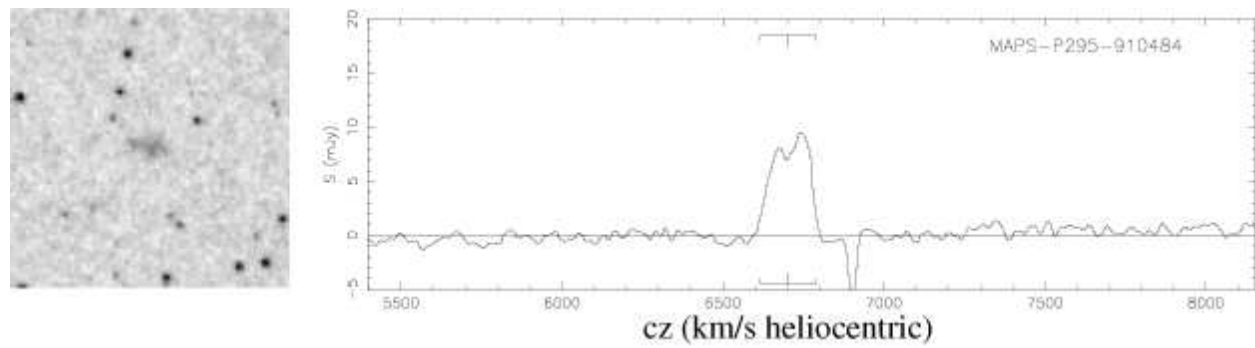


Figure 3 (Continued)

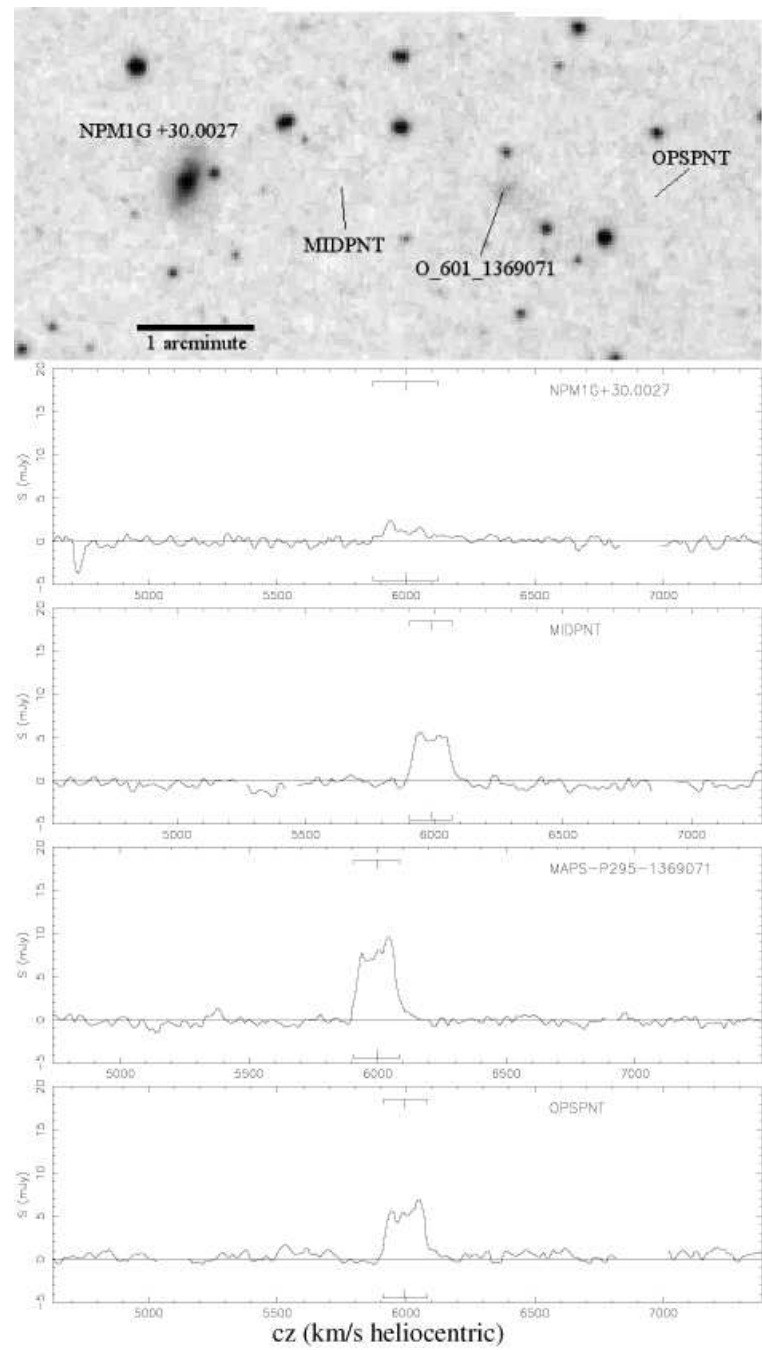


Figure 4

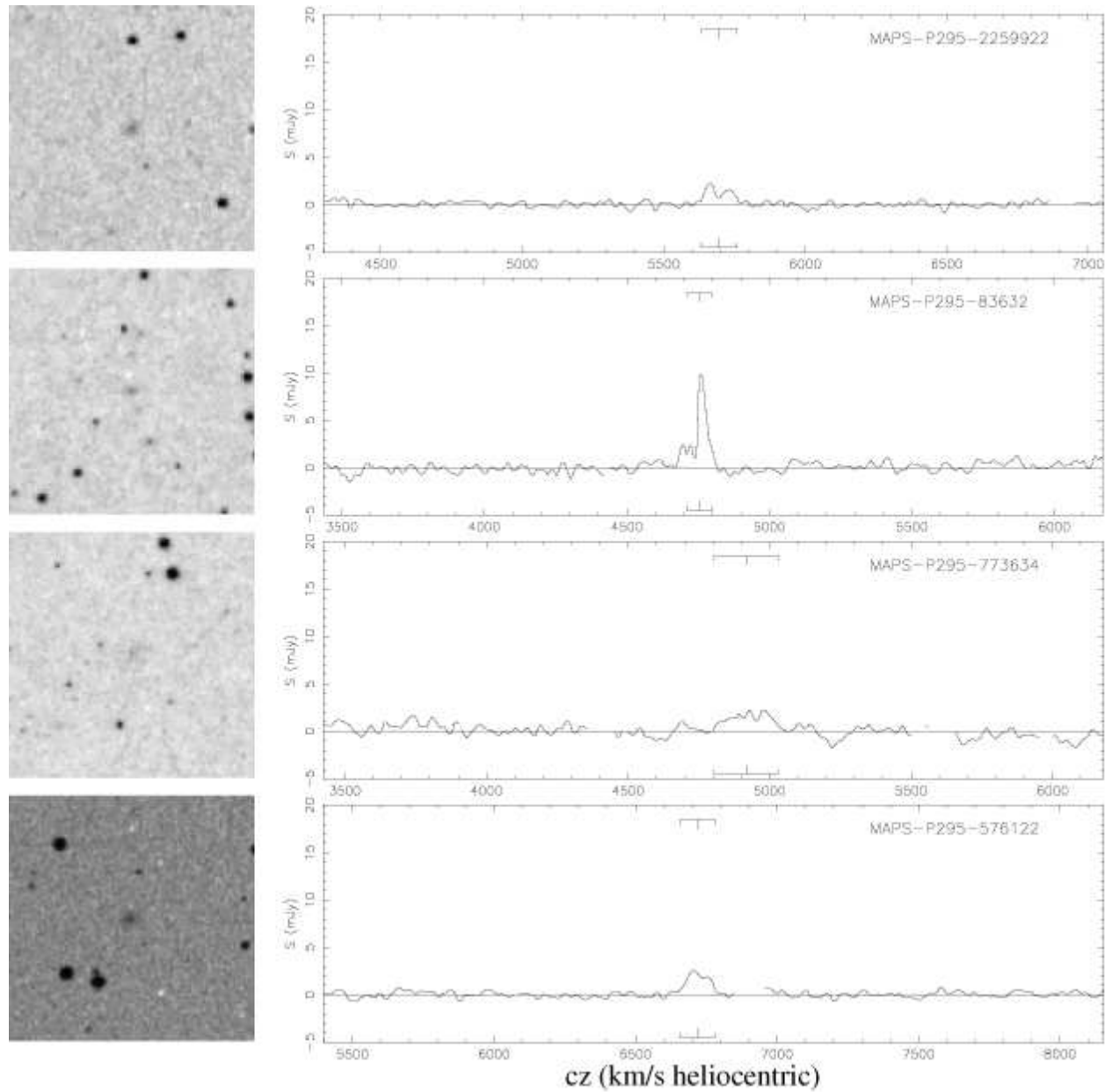


Figure 5

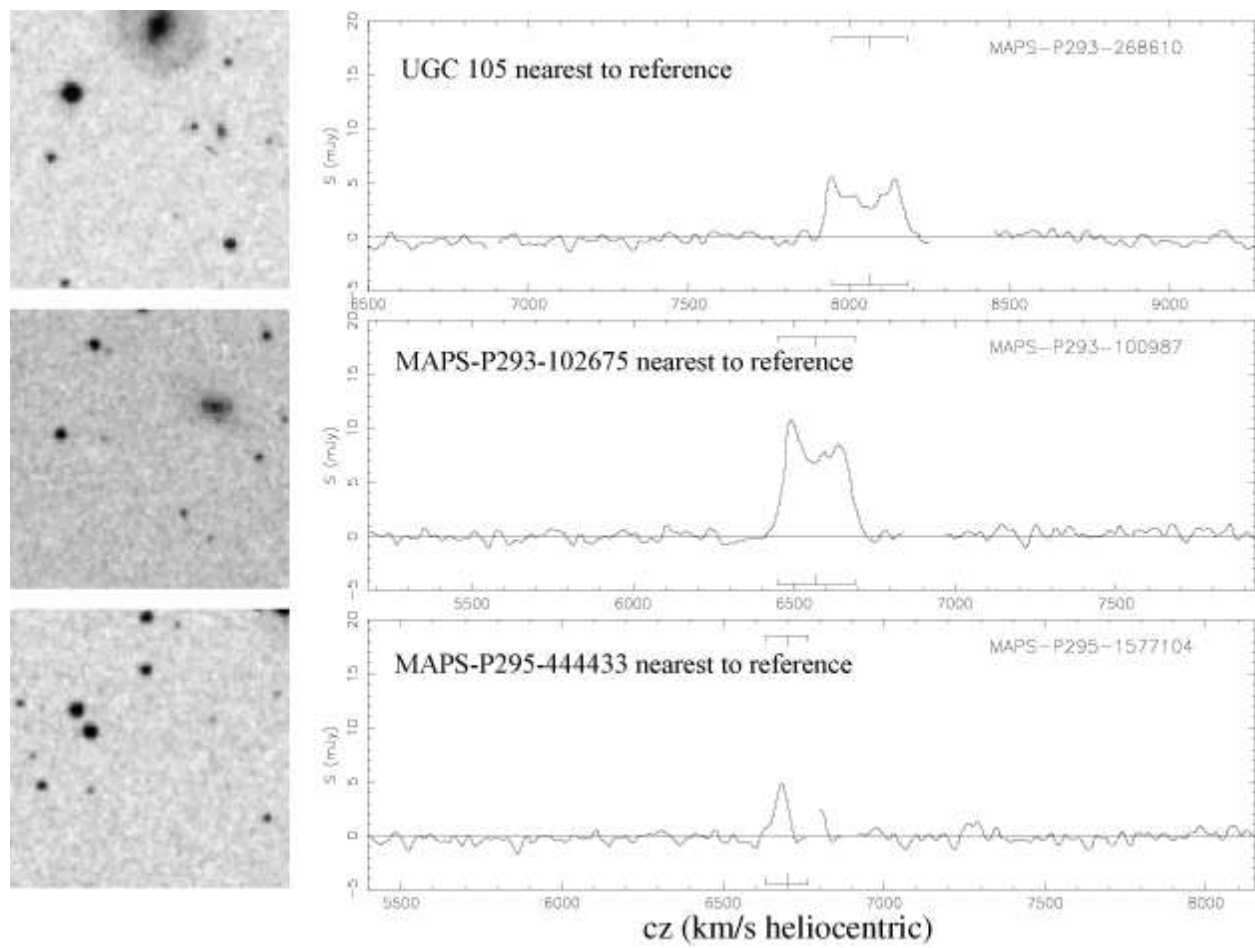


Figure 6

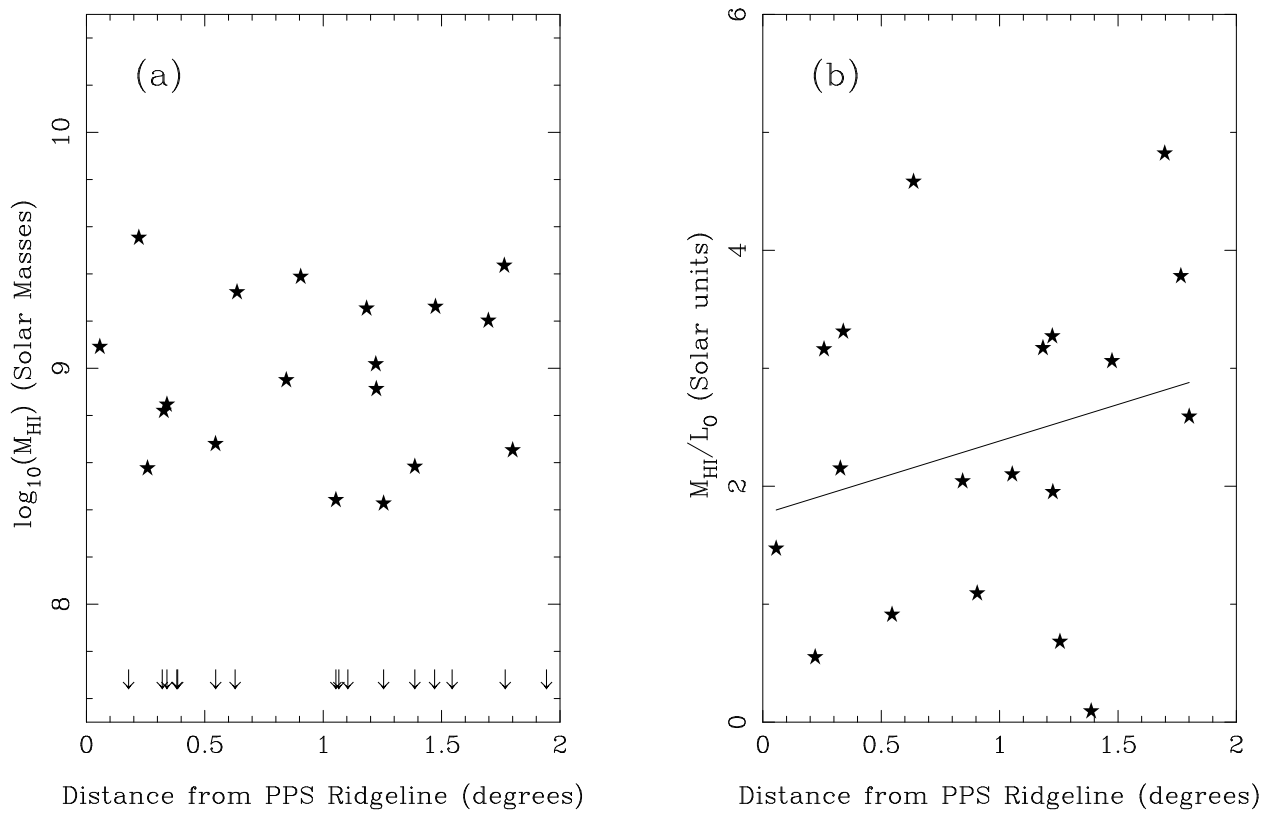
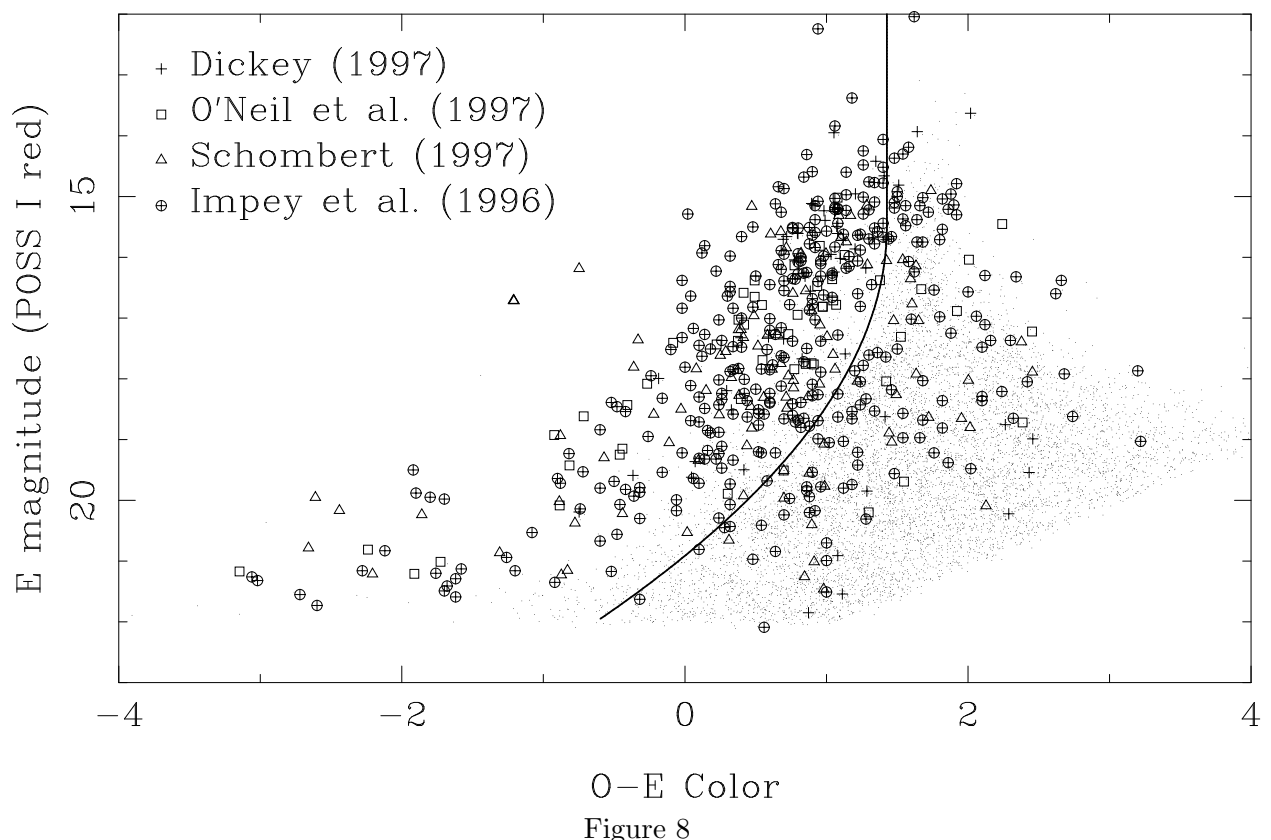
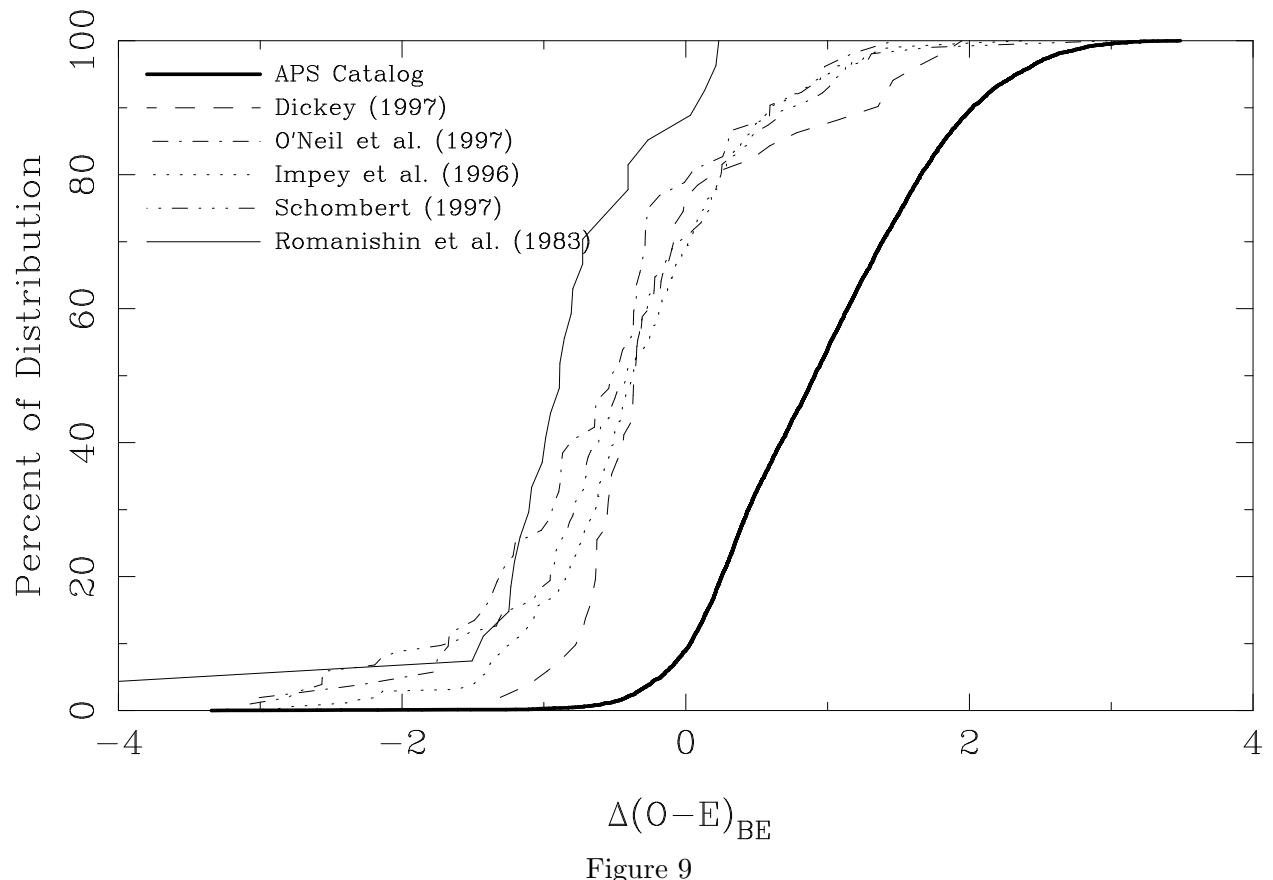


Figure 7





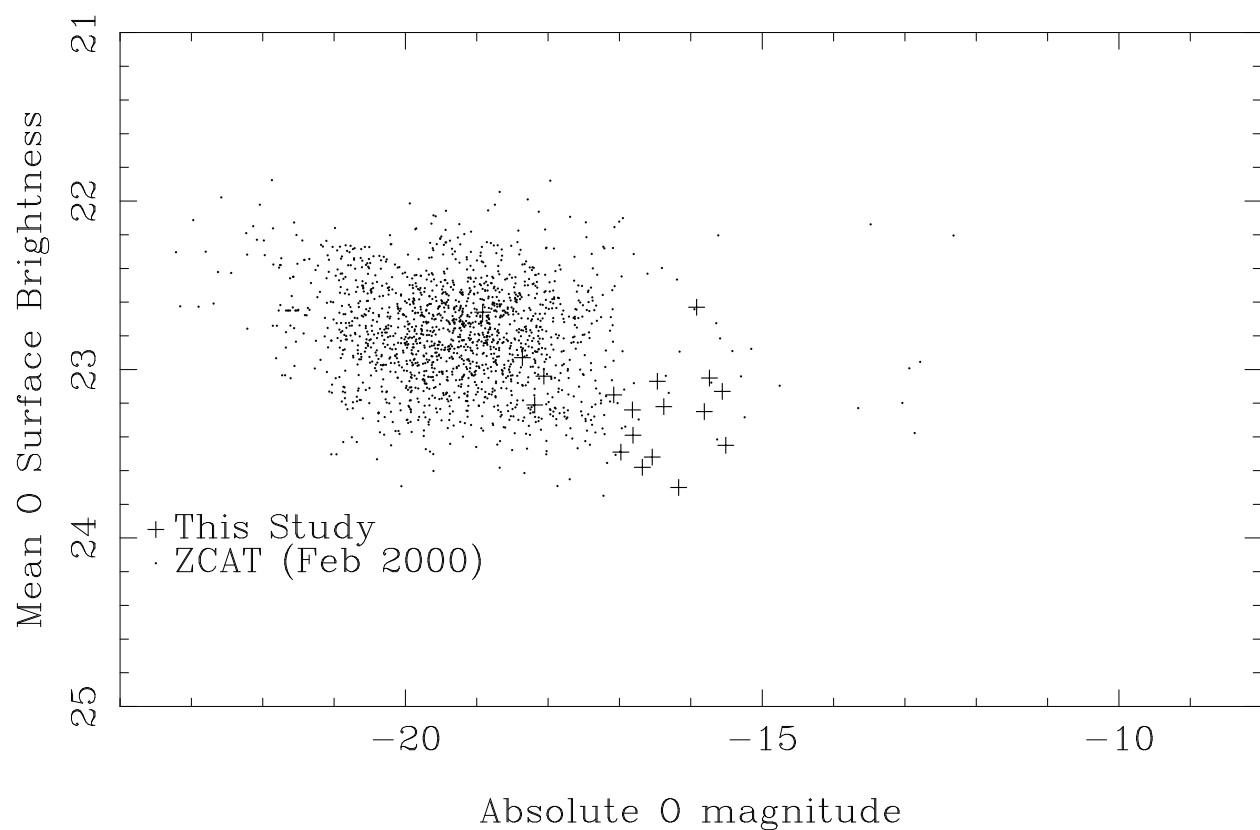


Figure 10

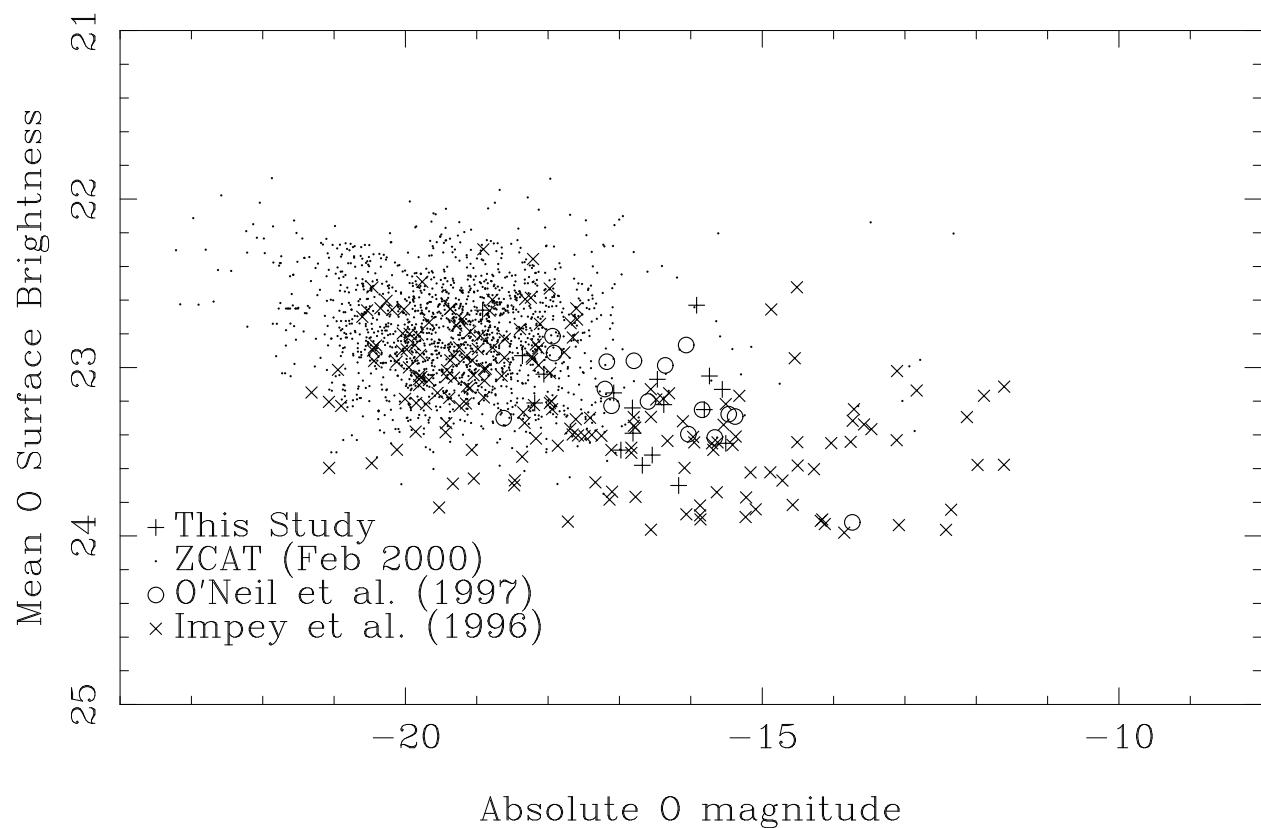


Figure 11

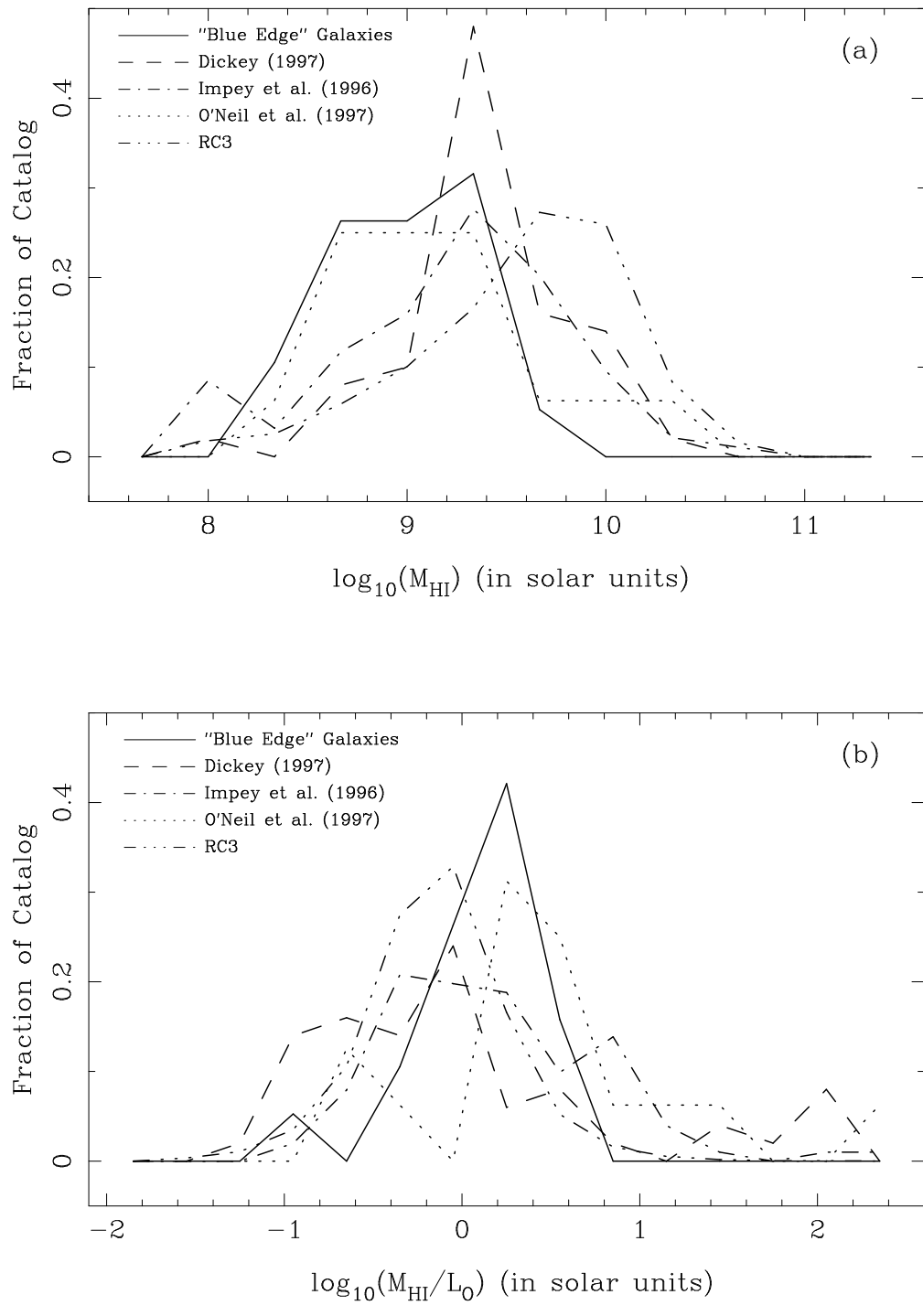


Figure 12

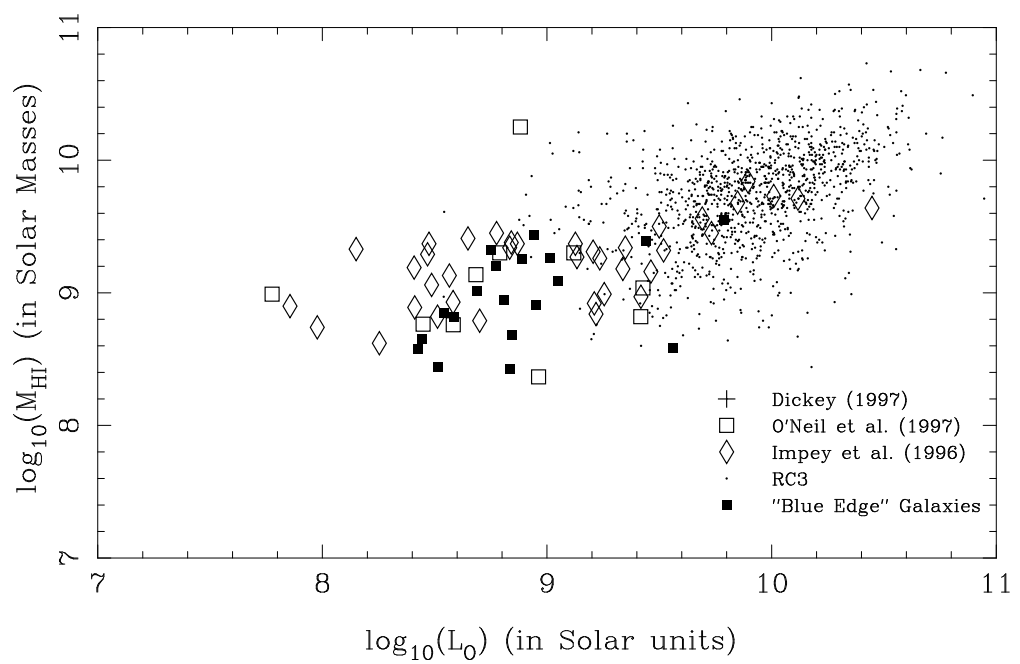


Figure 13

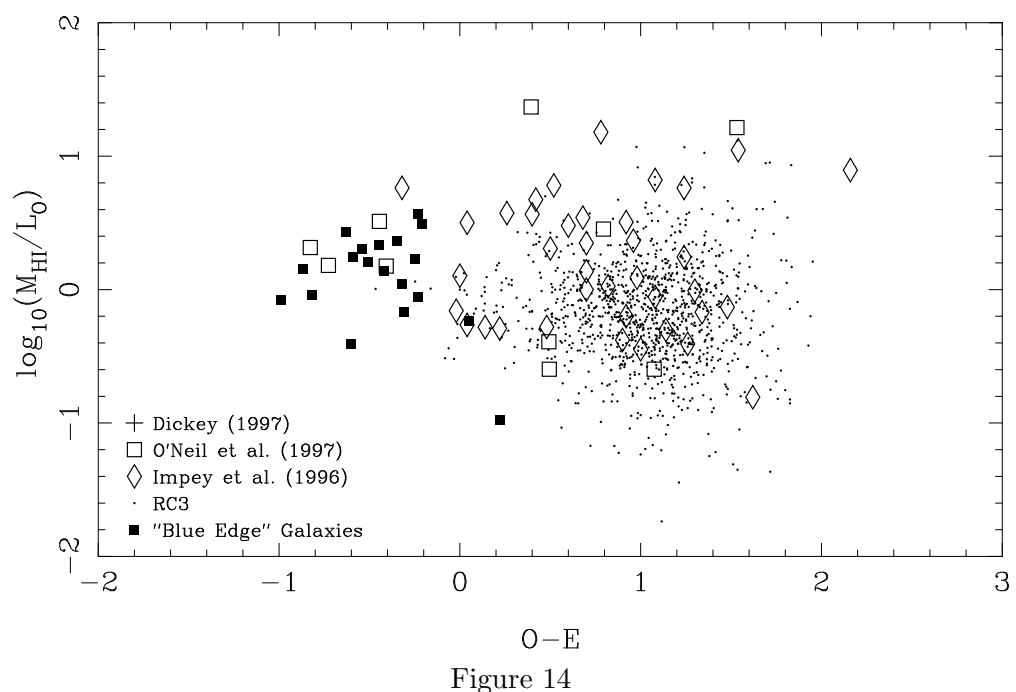


Figure 14

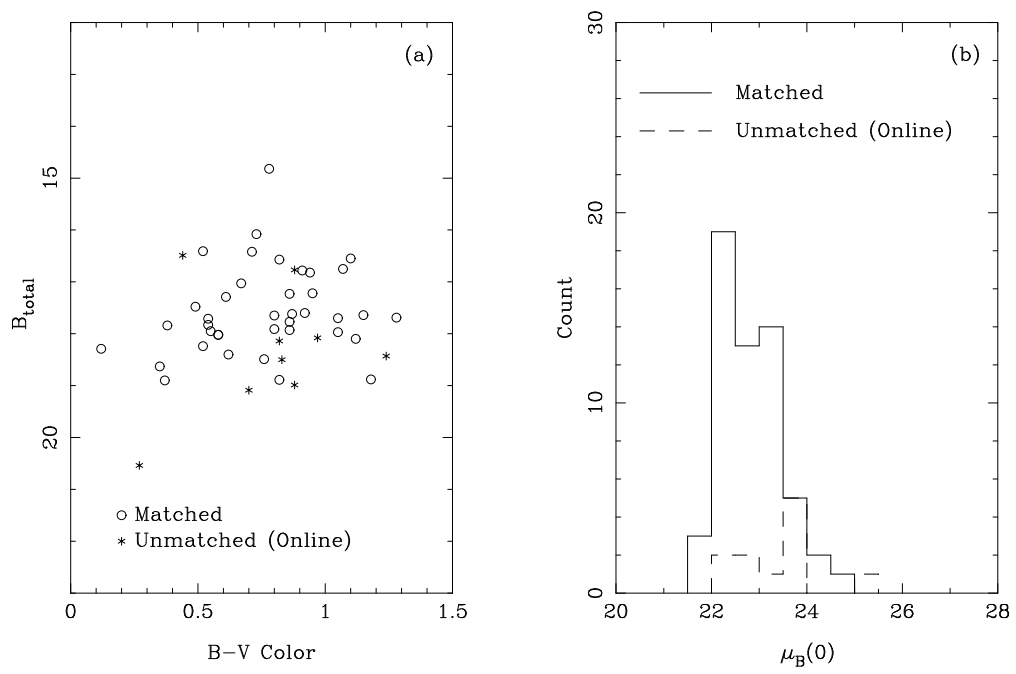
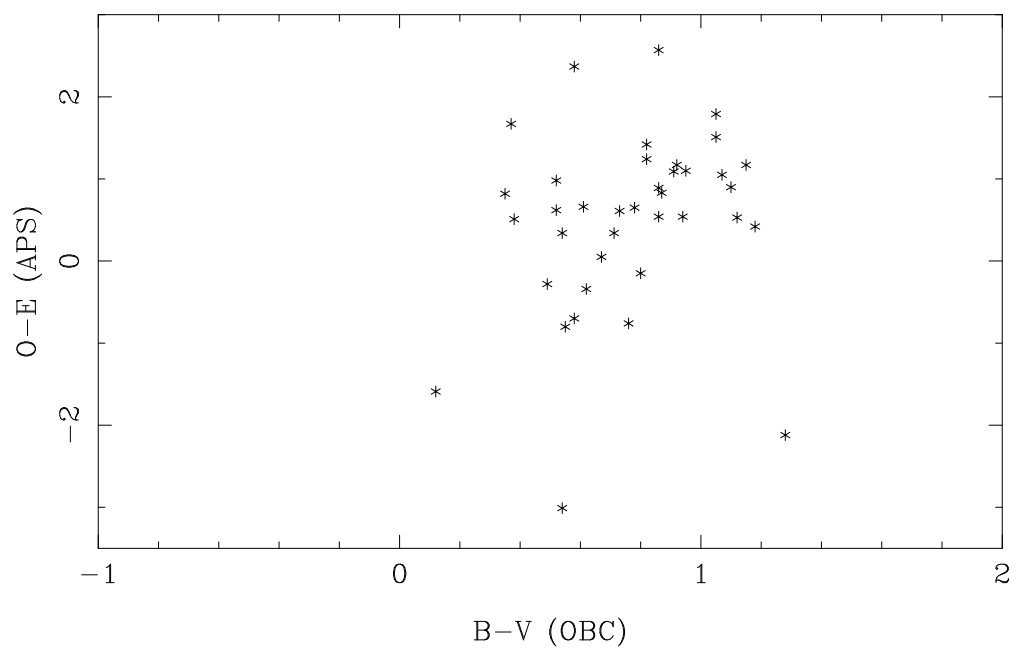


Figure 15



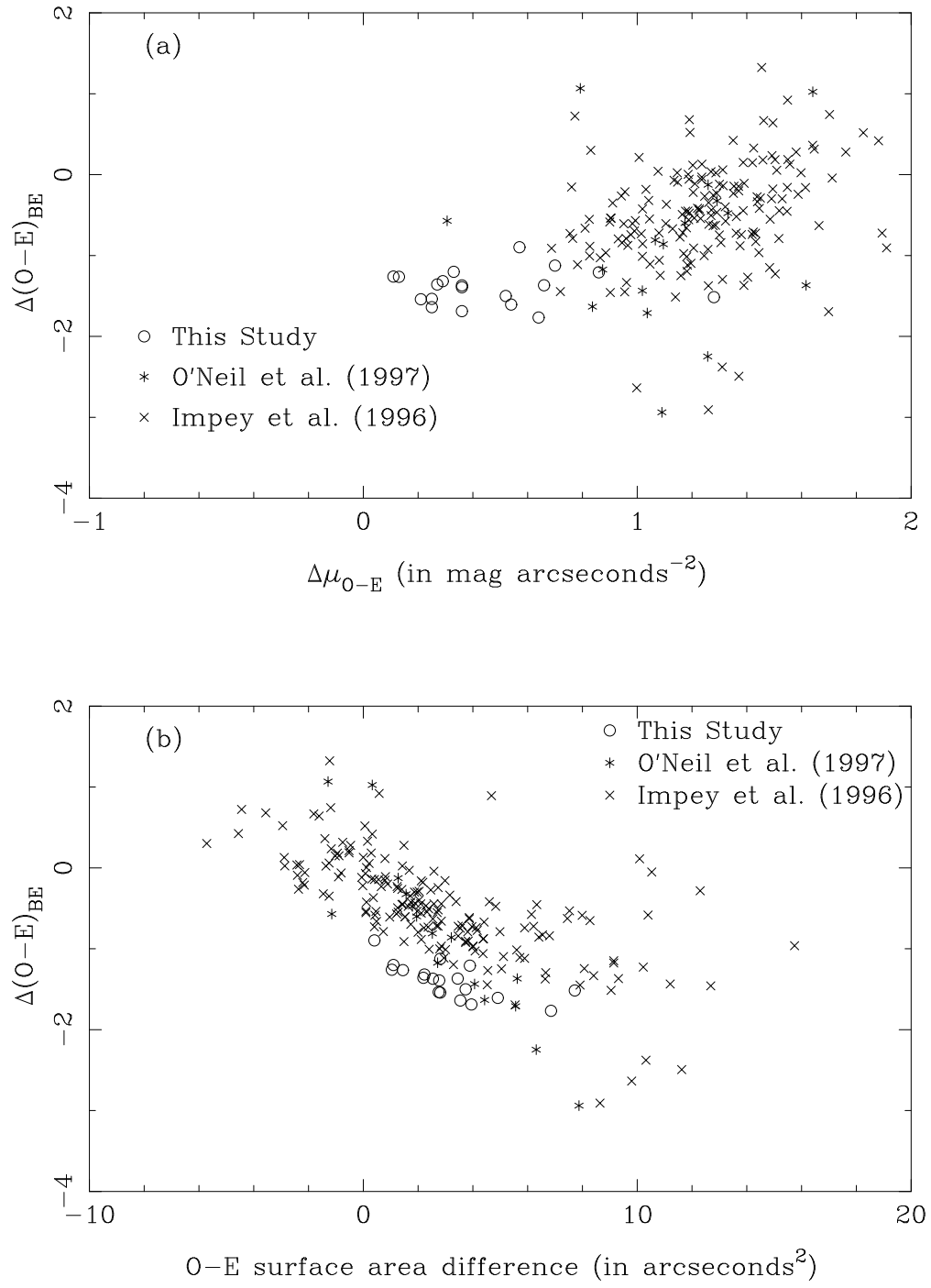
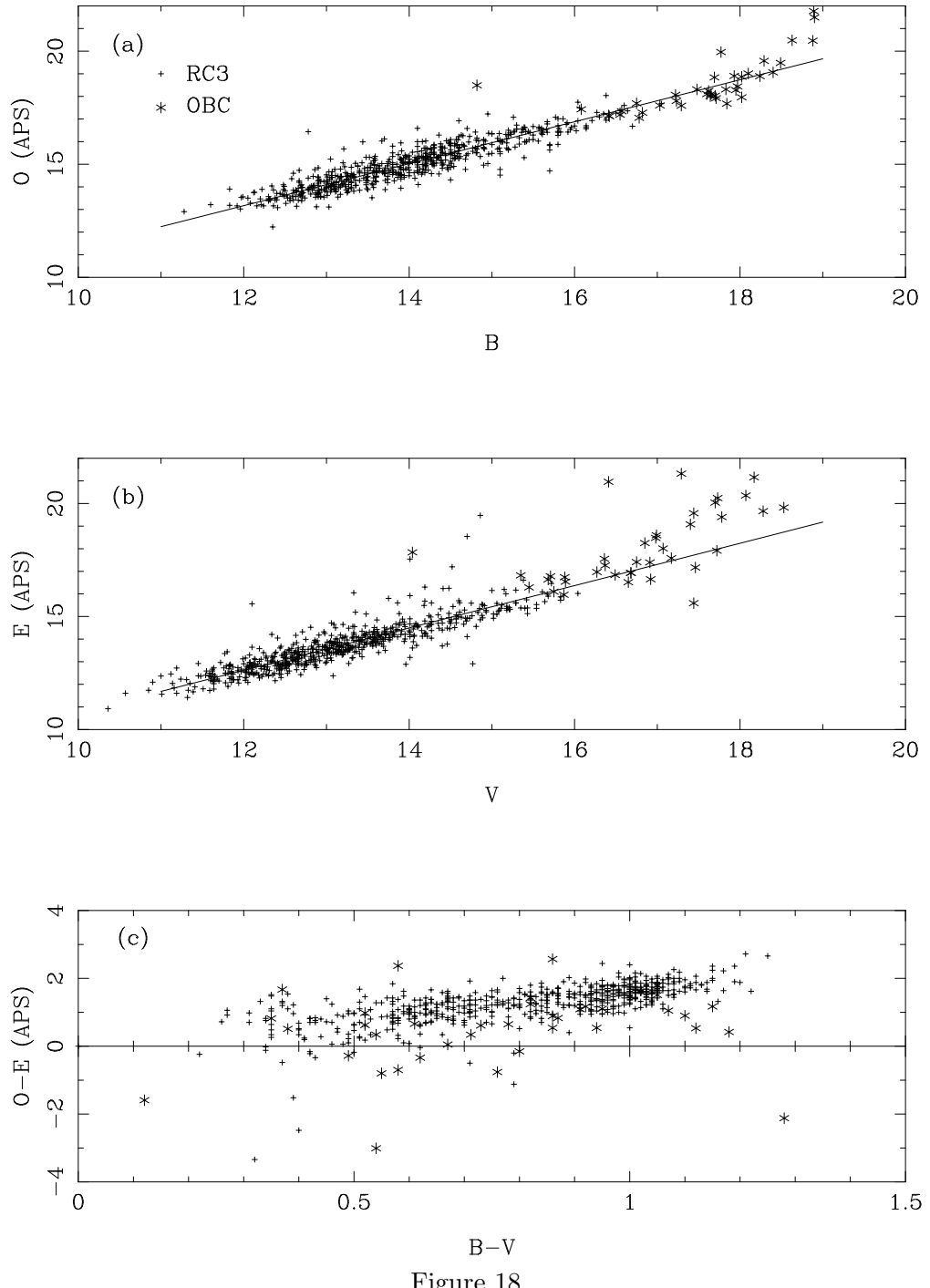


Figure 17



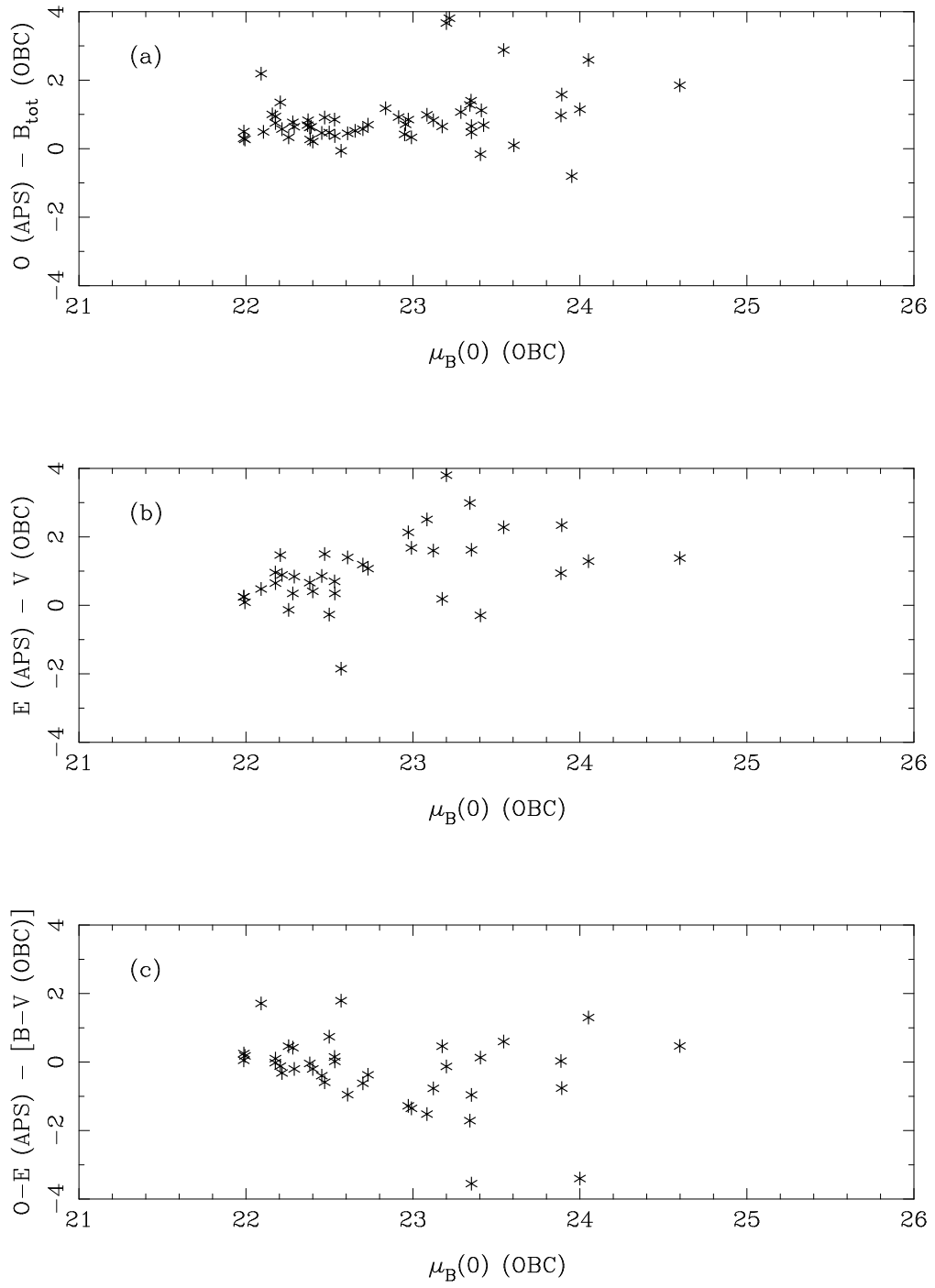


Figure 19